ORIGINAL PAPER

Mechanical stimulation of cell microenvironment for cardiac muscle tissue regeneration: a 3D in-silico model

Pau Urdeitx[1,2,3] · Mohamed H. Doweidar[1,2,3]

Abstract

The processes in which cardiac cells are reorganized for tissue regeneration is still unclear. It is a complicated process that is orchestrated by many factors such as mechanical, chemical, thermal, and/or electrical cues. Studying and optimizing these conditions in-vitro is complicated and time costly. In such cases, in-silico numerical simulations can offer a reliable solution to predict and optimize the considered conditions for the cell culture process. For this aim, a 3D novel and enhanced numerical model has been developed to study the effect of the mechanical properties of the extracellular matrix (ECM) as well as the applied external forces in the process of the cell differentiation and proliferation for cardiac muscle tissue regeneration. The model has into account the essential cellular processes such as migration, cell–cell interaction, cell–ECM interaction, differentiation, proliferation and/or apoptosis. It has employed to study the initial stages of cardiac muscle tissue formation within a wide range of ECM stiffness (8–50 kPa). The results show that, after cell culture within a free surface ECM, cells tend to form elongated aggregations in the ECM center. The formation rate, as well as the aggregation morphology, have been found to be a function of the ECM stiffness and the applied external force. Besides, it has been found that the optimum ECM stiffness for cardiovascular tissue regeneration is in the range of 29–39 kPa, combined with the application of a mechanical stimulus equivalent to deformations of 20–25%.

Keywords In-silico · 3D model · Cardiac muscle tissue · Cardiomyocyte · Mechanical stimuli

1 Introduction

Nowadays, cardiovascular diseases are the first cause of human death [1]. Due to the unrecoverable nature of the cardiac tissues, the damage suffered after the myocardial infarction has a particular importance [2]. The cardiac insufficiency produced by this deficiency or by other reasons may

✉ Mohamed H. Doweidar
  mohamed@unizar.es

1   Mechanical Engineering Department, School of Engineering and Architecture (EINA), University of Zaragoza, Zaragoza, Spain

2   Aragon Institute of Engineering Research (I3A), University of Zaragoza, Zaragoza, Spain

3   Biomedical Research Networking Center in Bioengineering, Biomaterials and Nanomedicine (CIBER-BBN), Zaragoza, Spain

produce a severe heart failure and even death. At present, the only effective method to restore heart functions is to subject the affected person to a heart transplant. However, at this time, the available healthy hearts for transplantation are insufficient to face the waiting lists [3]. The severity of the consequences reveals the importance of achieving an alternative technique to deal with these diseases. In this line, the scientific community has made a great effort to understand the morphogenesis processes of the cardiac tissues in order to be able to fabricate tissue fragments and recently whole the organ in-vitro. The possibility of making functional cardiac tissues in-vitro opens a new line of investigation with unlimited possibilities and a promising future.

To achieve an efficient cell culture for cardiac tissue regeneration, it is compulsory to understand the cellular behavior as well as the cues and stimuli needed for the morphogenesis process. If any of these factors is not correctly controlled and well-tuned, some vital aspects such as tissue architecture [4–6], cell phenotype [7] or cellular adhesion [8] may be altered and it could have a negative impact on the functionality of

the generated tissue [9]. In such cases, this generated tissue is not prepared to be used in-vivo.

Up to date, a large number of studies have been carried out for in-vitro development of cardiac tissues [7,10–12]. The construction of this type of tissue relies on clear advantages offered by stem cells to obtain autologous tissues [13]. In this context, very promising experimental studies have been developed, where a complete differentiation into cardiomyocytes has been achieved from different pluripotent cell resources [9,14,15]. Unfortunately, the regeneration of perfectly functional tissues has not been achieved. In most cases, electrically active tissues that mimic the original living tissues are obtained [16], and tissues with the capacity of spontaneous contraction are even generated [17]. However, the contractile stresses developed by these tissues are usually less than those that are developed in adult cardiac tissues [15,18]. This difference could be due to several factors, such as the lack of vascularization and innervation of the tissue or the state of differentiation and maturation achieved by the cells [19]. This deficiency of the generated tissue encouraged the scientific community to deepen its studies on cardiac tissue regeneration. Supporting the exerted experimental efforts with theoretical and computational models could be the best strategy to study these processes and find the optimal conditions for tissue regeneration.

Accordingly, in recent years, the development of computational models to explain, optimize and substitute an important part of the experimental work, has increased. Their clear advantages make possible to perform a large number of in-silico experiments to evaluate the effects of different parameters with a wide range of possible values. These models make possible to reduce dramatically the number of in-vitro and in-vivo experiments, with the consequent economic, time and pain saving.

From the computational point of view, two different approaches can be applied when addressing such models: discrete models, where single-cell interactions can be defined, and continuum models, where global behavior of cell populations is considered. Continuous models, usually based on cell densities, are suitable for studying the behavior of large cell populations, with a low computational cost. Using these models, it is easy to study some processes such as wound healing [20], nutrient consumption [21,22], scaffold design [23,24], etc. However, these models tend to simplify the physics of cell interaction and, in many cases, cell migration, which are essential to the definition of cellular structure in tissues. For instance, several studies have been shown that cell architecture is an important factor in tissue functionality. So it should be considered in the study of tissue regeneration [6,25–28]. Single-cell models can analyze the decisions made by each individual cell considering its specific environment, including ECM signals, cell–cell interactions, and cell–ECM interactions, and establish their relationship with

respect to the different cellular processes such as migration, proliferation, and apoptosis.

In 2004, Ramtami et al. [29] presented a new computational model to describe cell mechanics based on cell–cell and cell–ECM interactions from a continuum approach. In their interesting work, local contractions of a cell population interact actively with the ECM, however, single-cell perspective should be taken into account to study the cell–cell interactions. Zaman et al. [30] based on the differences observed between 2D and 3D in-vitro cultures, purposes one of the first 3D mechanical models for cell migration. In their work, several parameters such as ECM stiffness, and ligand density are considered in cell migration, and differences between 2D and 3D cell migration are exposed. Later, the developed computational models evaluate cellular behavior through an analysis of the stresses that they exert to sense their environment [31], studying processes such as 3D migration [32], protrusion generation [33,34], morphology [35–38] or even cellular differentiation [39].

Some recent works consider the adoption of stochastic approaches to define some cell parameters. For instance, some authors considered that cell protrusion could be given by molecular and thermal fluctuations, and purposes stochastic approaches for their study [34,40]. Nonetheless, stochastic models are usually limited by their computational cost and considering a large number of cells becomes computationally expensive (see interesting review in [41]). In this paper, we focused on the effect of the mechanical stimulation, and the effects of thermal and molecular fluctuations are considered as a randomness factor in the definition of the protrusion forces. In this point, deterministic models can give some advantages in terms of simplicity and from the computational point of view. So, we purpose a single-cell model with deterministic approach, that lets us simulate cell–cell and cell–ECM interactions in considerable populations of cells with reasonable computational costs. With this model, processes such as cell migration, differentiation, proliferation, apoptosis, cell–cell, and cell-matrix interaction, and the formation of specific cellular architectures have been studied.

2 Materials and methods

In the present work, a 3D computational model has been developed to study the cellular response to different stimuli. In particular, the processes of migration, differentiation, proliferation, and apoptosis of mesenchymal stem cells (MSC) as well as cardiomyocytes (CM). Besides, the model considers cell–cell and cell–ECM interactions, which can be experienced by the cells. Using the established model, the effect of different mechanical conditions, such as ECM stiffness and/or ECM applied external forces, can be evaluated
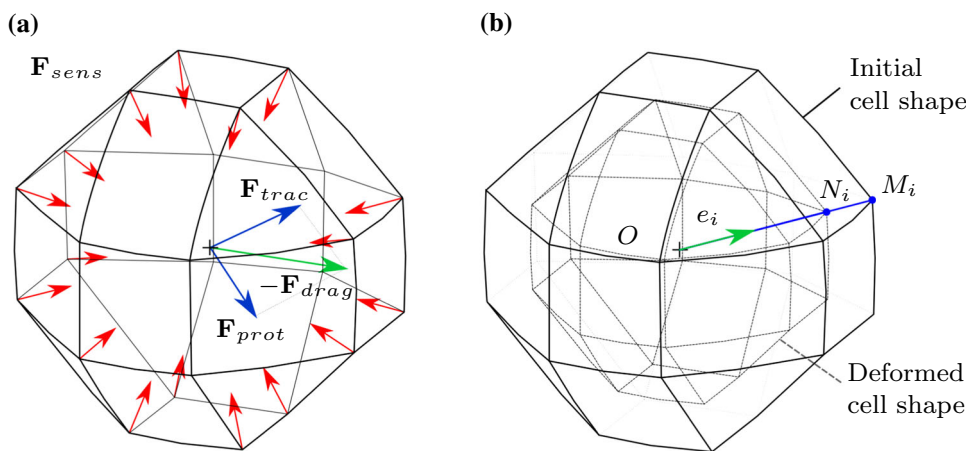
(a)

(b)

Fig. 1 Cellular mechanosensing and generated forces. **a** To explore its environment, the cell exerts some sensing forces, $\mathbf{F}_{sens}$, on the membrane nodes. The balance of forces is calculated in the cell centroid considering the traction force, $\mathbf{F}_{trac}$, protrusion force, $\mathbf{F}_{prot}$, and drag force, $\mathbf{F}_{drag}$. **b** Exerted cell stresses are proportional to the internal cell deformations. The internal cell deformation in the direction of e_i is established by the initial position vector of the ith node, OM_i, and deformed one, ON_i, the resulting length variation at the ith node is defined by the N_iM_i segment

to qualitatively study their effects on the development of the cell vital processes.

2.1 Cell migration

Cell migration plays a key role in many biological processes such as tissues regeneration or remodeling [42,43], wound healing [44] and cancer development [45–47]. Through mechanotaxis, the cell is able to interact with its ECM to evaluate the mechanical conditions of its microenvironment. Aspects such as ECM rigidity or the presence of other neighbor cells influence directly the cell decision to migrate towards a specific location. It can even guide the cells to regenerate a specific cell pattern to recover the original tissue functionality [2,5,25,48].

In the present model, during cell migration, a balance of forces is considered on the cell body. The considered forces are the traction force, $\mathbf{F}_{trac}$, generated by the cell Actin–Myosin (AM) apparatus, protrusion force, $\mathbf{F}_{prot}$, due to the expansion–retraction of the cell protrusions, and drag forces, $\mathbf{F}_{drag}$, due to the viscous resistance of the medium to cell movement (Fig. 1a). Here, the inertial effects are negligible in comparison with the rest of the considered forces. In this way, the balance of forces can be defined as [49]:

$$\mathbf{F}_{trac} + \mathbf{F}_{prot} + \mathbf{F}_{drag} = 0. \tag{1}$$

Traction forces, $\mathbf{F}_{trac}$, are transmitted through the cell adhesion located in the cell membrane. So, the traction force, given by the resultant of the forces applied in each membrane node in the discretized cell, can be calculated as:

$$\mathbf{F}_{trac} = \sum_{i=1}^{n} \mathbf{F}_i^{trac}, \tag{2}$$

where $\mathbf{F}_i^{trac}$ is the traction force applied at each ith node of the cell, and n is the number of external nodes of the cell. These nodal traction forces are calculated through the internal cell stresses as:

$$\mathbf{F}_i^{trac} = \sigma_i \, S \, \zeta \, \mathbf{e}_i, \tag{3}$$

where σ_i is the exerted stress on the ith node, $\mathbf{e_i}$ is the direction of that node with respect to the center of the cell, S is the node proportional cell surface area and ζ is a dimensionless parameter related to the adhesiveness of the cell. This parameter takes into account the density of ligands on the cell surface, ψ, the number of available receptors in the cell, n_r, and the binding constant, k. It can be calculated by [30]:

$$\zeta = k \, n_r \, \psi. \tag{4}$$

The cell exerted stresses, σ_i, are considered to be dependent on the internal cell strains, ε_i. These stresses can be classified into two groups: active stresses, generated by the actin–myosin filaments contraction, and passive stresses, generated by the resistance of the cell membrane and the cytoskeleton to be deformed (Fig. 2a). It is supposed that the actin–myosin crosslinking motor system generates stresses directly proportional to the internal deformation experimented by the cell due to the exerted sensing forces, $\mathbf{F}_{sens}$. The generated internal cell deformation is considered to be bounded by the maximum deformation, ε_{max}, and minimum deformation, ε_{min} (Fig. 2b). In a similar way, the passive
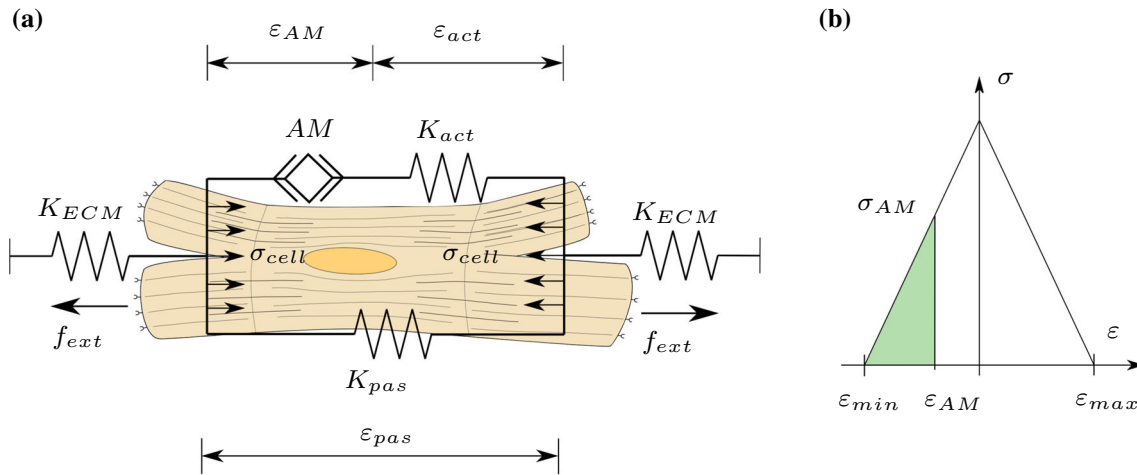
Fig. 2 Cellular mechanosensing model. **a** Mechanical model of the cell. The contraction of the Actin–Myosin machinery, *AM*, generates stresses that are transmitted to cell adhesions through the cytoskeleton, which generates active, ε_{act}, and passive, ε_{pas}, deformations on the cell elements, as well as the ECM deformation, ε_{ECM}. σ_{cell} represents the stresses resulting from the *AM* contraction and the resistance to deformation of the active, K_{act}, and passive, K_{pas}, elements, where K_{act} and K_{pas} are the stiffness modulus of actin filaments and the passive components of the cell, respectively. Likewise, K_{ECM}, is the ECM stiffness. f_{ext} is an applied external force. **b** Cell exerted stresses generated by the actin–myosin machinery, σ_{AM}, which are linearly dependent on ε_{AM}. ε_{min} and ε_{max} are minimum and maximum cell internal deformation, respectively

stresses are considered to be dependent linearly on the internal cell deformation. So, the cell exerted stresses can be calculated by [39]:

$$
\sigma_i =
\begin{cases}
K_{pas}\,\varepsilon_i & \varepsilon_i < \varepsilon_{min} \text{ or } \varepsilon_i > \varepsilon_{max} \\[2mm]
\frac{K_{act}\sigma_{max}(\varepsilon_{min}-\varepsilon_i)}{K_{act}\varepsilon_{min}-\sigma_{max}} + K_{pas}\,\varepsilon_i & \varepsilon_{min} \leq \varepsilon_i \leq \tilde{\varepsilon} \\[2mm]
\frac{K_{act}\sigma_{max}(\varepsilon_{max}-\varepsilon_i)}{K_{act}\varepsilon_{max}-\sigma_{max}} + K_{pas}\,\varepsilon_i & \tilde{\varepsilon} \leq \varepsilon_i \leq \varepsilon_{max}
\end{cases}
$$

(5)

ε_i can be calculated at each external node of the cell considering the variation of the radius with respect to its initial value as (Fig. 1b):

$$
\varepsilon_i = \frac{N_i M_i}{O M_i}.
$$

(6)

K_{pas} and K_{act} are the active and passive stiffness of the cell, respectively (Fig. 2a). σ_{max} is the maximum stress generated by the actin–myosin machinery, which is related to the contraction capability of the Actin–Myosin machinery, ε_{AM}. As the AM deformation is strongly coupled to the active, ε_{act}, and passive, ε_{pas}, deformations, it is complicated to obtain. However, this deformation is the generator of the motor forces of the cell, being implicitly contained in σ_{max}. Finally, $\tilde{\varepsilon}$, is the result of establishing a linear approximation of the cell internal stresses between ε_{min} and ε_{max}, defined as:

$$
\tilde{\varepsilon} = \sigma_{max}/K_{act}.
$$

(7)

Protrusion forces are generated by the expansion and retraction of protrusions of the cell. These protrusions are generated randomly by the polymerization and depolymerization of cell actin filaments. They generate new anchor points that alter the migration direction. The magnitude and direction of these forces will depend on the size and location of the generated protrusions, the magnitude is always less than the traction forces. So, the protrusion forces can be defined as:

$$
\mathbf{F}_{prot} = \kappa \parallel \mathbf{F}_{trac} \parallel \mathbf{e}_{rand},
$$

(8)

where κ is a random value between $0 \leq \kappa < 1$, and e_{rand} is a random unit vector.

Finally, the drag force, $\mathbf{F}_{drag}$, is the needed force to penetrate the cell within the ECM. This force has been calculated by applying the Strokes law, considering the cell as a spherical element with r radius moving at a $\mathbf{v}$ velocity in a medium with a η viscosity [50].

$$
\mathbf{F}_{drag} = 6\,\pi\,r\,\eta\,\mathbf{v}.
$$

(9)

So, solving the Eq. (1), the migration speed, $\mathbf{v}$, and the cell displacements, $\mathbf{d}$, can be calculated at time t by

$$
\mathbf{d} = \frac{\mathbf{F}_{drag}}{6\,\pi\,r\,\eta}\,t.
$$

(10)

2.2 Cell–cell interaction

Cell interactions play a key role in cell behavior. Cells in contact may change drastically their behavior on such aspects as cell proliferation [66,67] and migration [44,68]. Along the contact surface between two cells, they lose the ability to generate protrusions, thus limiting the ability to interact with the ECM. Likewise, this allows cells to establish intercellular connections to develop their collective activities. In the case of muscle cells, cells are grouped to form chains (fibers) conveniently oriented acquiring the ability to transmit contractile forces collectively in a preferred direction, which requires that the orientation of their cytoskeleton (forming sarcomeres) are consistent with the direction of the cell binding.

In the present model, these complex cell–cell interactions have been considered and implemented. First, an overlapping limitation has been established so that interference between cells is not allowed during the cell migration. So, for any pair of cells, the distance between them must satisfy the criterion of non-interference. Being $\mathbf{X}_i$ and $\mathbf{X}_j$ the position vector of the cells ith and jth, respectively, the distance between them, $\mathbf{X}_{ij}$, is calculated as:

$$\mathbf{X}_{ij} = \mathbf{X}_j - \mathbf{X}_i. \tag{11}$$

To establish the non-interference criterion, cells are considered to fulfill all the time that $\| \mathbf{X}_{ij} \| \geq 2r$ (Fig. 3a). Consequently, if two cells are in contact, the cell contact direction can be calculated as:

$$\mathbf{e}_{ij} = \frac{\mathbf{X}_{ij}}{\| \mathbf{X}_{ij} \|}. \tag{12}$$

The effect of cell adhesion has also been considered. This adhesion will be conditioned by the orientation of the cells with respect to the contact direction. The orientation of the cell is dependent on the direction of the cytoskeleton of the cell. This direction will be defined as the direction of the minimum deformation of the cell after the mechanosensing process, as:

$$\mathbf{e}_{pol}^i = \frac{1}{n} \sum_{j=1}^n \varepsilon_j \, r \, \mathbf{e}_j, \tag{13}$$

where ε_j is the internal deformation, r is the radius of the cell and $\mathbf{e}_j$ is the position vector, at the jth node of the ith cell.

Besides, we have defined a global polarization direction ($\mathbf{G}_{pol}$), which has the direction of the resultant of all the individual cell's polarization direction after the mechanosensing process to monitor the general direction of cell polarization at every time step (Fig. 3b). So, $\mathbf{G}_{pol}$ is calculated as:

$$\mathbf{G}_{pol} = \frac{\mathbf{R}_{pol}}{\| \mathbf{R}_{pol} \|}, \tag{14}$$

where

$$\mathbf{R}_{pol} = \frac{1}{n} \sum_{i=1}^n \frac{\mathbf{e}_{pol}^i}{\| \mathbf{e}_{pol}^i \|}. \tag{15}$$

In the present model, if two cells are in contact, it is considered that they generate a stable attachment to form a muscle fiber if the following two conditions are satisfied (1) two or more nodes in the discretized cell's membrane are in contact and (2) the cell contact direction agrees with the $\mathbf{G}_{pol}$ within an established range. For this purpose, the cell contact direction, $\mathbf{e}_{ij}$, is projected on $\mathbf{G}_{pol}$ and then is divided by the longitude of $\mathbf{G}_{pol}$, as:

$$l_{ij} = Proj(\mathbf{e}_{ij}, \mathbf{G}_{pol}), \tag{16}$$

l_{ij} is a value between 0 and 1 which gives insight on the proximity of these two directions. In this way, if the two vectors have the same direction then $l_{ij} = 1$, meanwhile, if they are in perpendicular directions then $l_{ij} = 0$. So, to define a stable contact, capable of forming a muscle fiber, l_{ij} should be within the following established range $1 \geq l_{ij} \geq l_{adh}$ (see Table 2) and $\| \mathbf{X}_{ij} \| = 2r$. The cells, which are joined in this way, tend to remain attached.

Unlike individual cell migration (Fig. 4a), cells will pull on each other, tending to drag all the group. Thereby, a collective response is generated where the joined cells move together (Fig. 4b). To reproduce this effect, for the cells that are considered part of a group, Eqs. (1)–(8) are calculated considering the whole group as one entity. Due to the irregular group shape, we have to change Eq. (9) by introducing a shape factor, f_{sh}, as [38]:

$$\mathbf{F}_{drag} = f_{sh} \, 6 \pi \, r_{grp} \, \eta \, \mathbf{v}_{grp}. \tag{17}$$

Here r_{grp}, and $\mathbf{v}_{grp}$, are the group's equivalent radius and velocity, respectively. Being l_{min}, l_{max}, and l_{med}, the minimum, maximum and medium lengths, respectively, representatives of the group's ellipsoid morphology, and taken with respect to an orthogonal reference system, the shape factor, f_{sh}, is calculated as [38]:

$$f_{sh} = \left[\frac{l_{max} \, l_{med}}{l_{min}^2} \right]^{0.09}. \tag{18}$$

Finally, applying Eq. (10), we obtain the group displacement, d_{grp}.

Besides, cells have the capacity of relocating spatially positions that are more favorable to them. Thus, although the cells move together, there is also a tendency to move them

Fig. 3 Cell interaction. **a** $\mathbf{X}_i$ and $\mathbf{X}_j$ are the position vector of the ith and jth cells, respectively, $\mathbf{X}_{ij}$ is a vector passing by the centroids of these two cells, which must satisfy $\parallel \mathbf{X}_{ij} \parallel \geq 2r$. ($n_1 : n_4$) are the common nodes. In these nodes, cells lose their capacity of exerting protrusions to interact with the ECM. **b** The global polarization direction, $\mathbf{G}_{pol}$, is calculated as the average of all cell polarization directions, e_{pol}^i. To establish the type of contact, l_{ij} is defined as the projection of $\mathbf{X}_{ij}$ in the $\mathbf{G}_{pol}$ direction
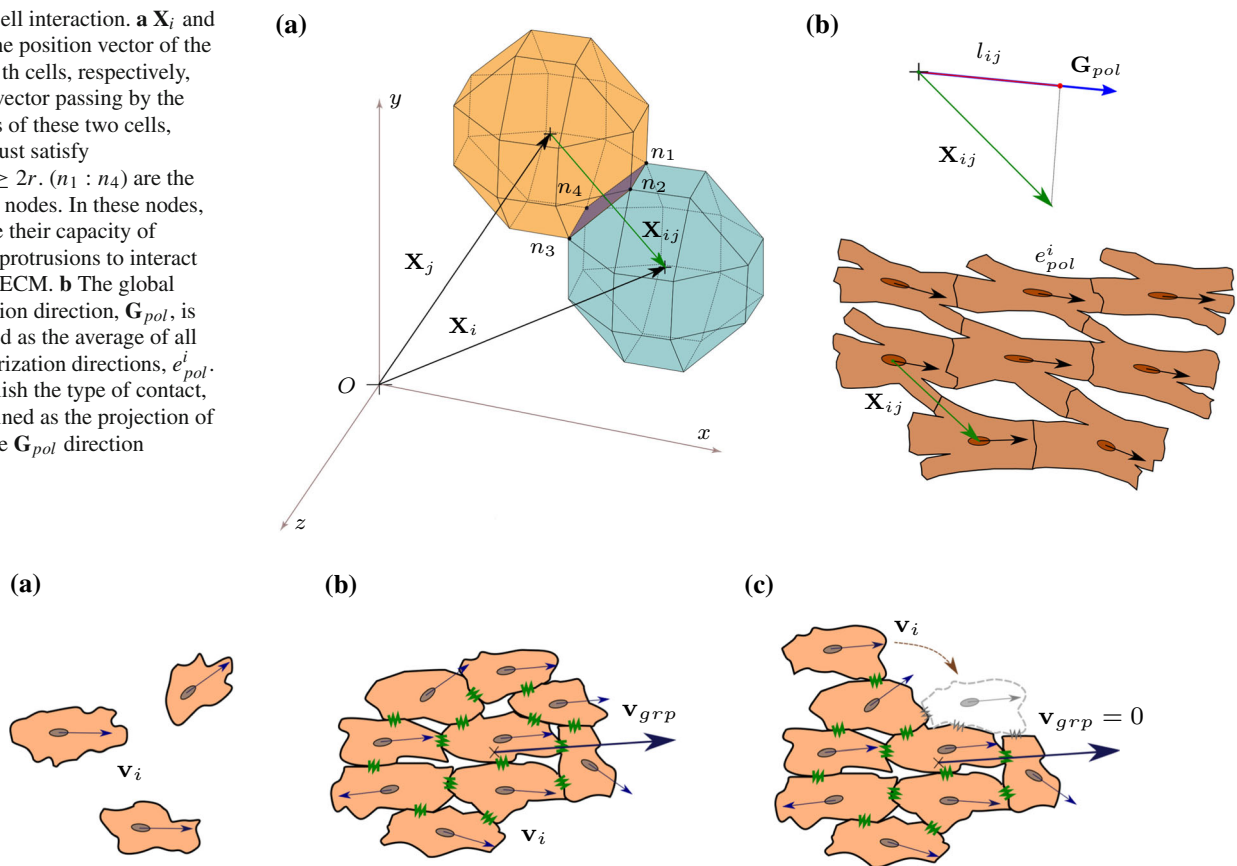
Fig. 4 Collective migration. Different cell behaviors are considered in cell migration. **a** Single-cell migration is considered when cells are separated, or they are not attached to any group of cells. **b** Collective cell migration is applied to any group of cells bonded together. Group translocation is a consequence of the interaction of each cell in the group with the EMC. **c** Cells also have the capacity of moving inside the group to improve their integration within the group

within the group (Fig. 4c), due to the interaction between them. However, during the same time-step of interaction, the possibility of a cell moving twice has been discarded. So, if a cell moves along with a group, it loses the ability to move independently. Moreover, if the group does not move during a determined time step, any cell in that group has the capability to relocate itself within the group, thus it can migrate to a new position. Displacement applied, in this case, will be the result of the evaluation of Eqs. (1)–(10) for that cell individually (see Fig. 4c).

2.3 Cell fate

Different studies have shown the relevance of the mechanical conditions of the cell environment in the differentiation of stem cells [70,75,76], as well as its maturation [7,18] and apoptosis [77,78]. Cultured MSCs are capable of mimicking different tissues, trigger the differentiation into the typical cellular phenotype of the mimicked tissue. Although the mechanotransduction pathways are multiple and remain

elusive, some advanced studies suggest that deformations in cell nucleolus as well as in specific proteins of the nucleus membrane can trigger specific biological processes [79,80]. This requires the communication of the deformations experienced in the cell membrane, which is sensing the mechanical microenvironment of the cell, to the cell nucleus through the cytoskeleton. Understanding and controlling the processes that trigger this differentiation can present a clear advantage in the treatment of different diseases. However, the complexity of the composition and properties of some tissues, such as cardiac tissue, presents a great challenge to overcome in order to produce in-vitro tissue constructs with comparable properties to in-vivo tissue. Stoppel et al. presented a review of the response of CM to mechanical and electrical stimuli, where the complexity of the mechanical conditions of the cellular environment and its implications during the fabrication of cardio-like constructs are exposed [69].

In the present work, the effects of ECM stiffness as the main promoter of cell differentiation will be considered. The stiffness of the ECM can be perceived by the cell through the

stresses or deformations that the cell membrane experiences. However, the relationship between stiffness and deformations is not always direct, and depends, among others, on the mechanical properties of the ECM and the boundary conditions. In this study, the mechanical behavior of the ECM has been considered as linear elastic. Under these conditions, the relationship between stresses and strains is known and direct. This allows us to define the mechanical stimulus as a function of the deformations of the ECM, which in turn will be related to the stiffness of the ECM. Thereby, the intensity of the mechanical stimulation received by the cell is calculated, as a consequence of the interaction of the cell with the medium, through the deformation of the cell membrane as:

$$\gamma_c(t) = \frac{1}{n} \sum_{i=1}^{n} \mathbf{e}_i : \boldsymbol{\epsilon}_i : \mathbf{e}_i^T, \tag{19}$$

where γ_c is the mechanical stimulus on the cell, $\boldsymbol{\epsilon}_i$ is the strain tensor at the ith node of that cell, $\mathbf{e}_i$ is the direction vector of the ith node respect to the center of the cell, and n is the number of the nodes in the cell membrane.

Considering the deformation experienced by the cell in ECMs with different stiffness, the ranges of mechanical stimulation that trigger the differentiation of a certain cellular phenotype can be obtained. The specific signal transduction pathway of the cell differentiation due to the mechanical stimulus is still unclear, however, it is known that the deformation experienced by the cell membrane can be transmitted through the cytoskeleton to the cell nucleus thus triggering the transcription of specific differentiation factors [73,81]. Besides, cells require a certain level of maturity to active the differentiation or proliferation processes. In this way, cell differentiation becomes a time-dependent process, requiring the application of a specific level of mechanical stimulation along the period of the cell maturation.

The time necessary to activate the differentiation, as well as the proliferation, depends on the cell type. It has been observed that the increase of the rigidity of the ECM can reduce the time necessary for the maturation of the cell, suggesting that cell maturation depends in a certain way on the level of stimulus that the cell receives [73,82]. Although this time can be reduced by the mechanical stimulus, the cell always needs a certain minimum time to trigger the processes of differentiation and proliferation [81]. Consequently, it is proposed that the maturation time of the cell can be calculated as:

$$t_{mat}(\gamma, t) = t_{min} + t_p \gamma_c(t), \tag{20}$$

where t_{mat} is the time necessary for the cell maturation, t_{min} is the minimum time needed to cell proliferation or differentiation, and t_p is a proportional time, which depends on the mechanical stimulus γ_c.

The maturation state of each cell can be defined through the Maturation Index (MI) calculated from the maturation time as:

$$MI = \begin{cases} \frac{t}{t_{mat}} & t \leq t_{mat} \\ 1 & t > t_{mat} \end{cases}. \tag{21}$$

The differentiation of stem cells, s, into cardiac myocyte cells, m, depending on the mechanical conditions of the ECM, has been considered. Thus, cell phenotype, $i \in \{s, m\}$, will be conditioned by the state of maturation (MI) as well as by the level of mechanical stimulus it receives. Thus, once an undifferentiated cell reaches MI $= 1$, if the level of mechanical stimulation is within the threshold of differentiation of a given cell type, the cell will be differentiated into the corresponding phenotype.

$$\text{Cell state} = \begin{cases} m & \gamma_{low} < \gamma_c \leq \gamma_{myo} \ \& \ MI = 1 \\ \text{apoptosis} & \gamma_{apop} < \gamma_c \\ \text{no differentiation} & \text{otherwise} \end{cases} \tag{22}$$

On the other side, cell proliferation plays a key role in tissue regeneration, allowing cells to replicate themselves to increase their number. For this purpose, cells go through several stages of growth before triggering mitosis, where the cell divides to generate two new cells instead [83]. The capacity of cell proliferation seems to be closely related to the level of differentiation of some lineages, the more specialized is the phenotype the lower is their proliferation capability, thus limiting the ability of natural regeneration of certain tissues [73,84]. It has also been observed that there is a close relationship between mechanical stimulation and proliferation, having observed the inhibition of cell proliferation under different mechanical conditions [66–68,85]. Thus, in the present model, the cell proliferation capacity has been implemented, relating it to the mechanical stimulation and the maturation time such as:

Cell proliferation
$$= \begin{cases} 1 \text{ mother} \to 2 \text{ daughter} & \gamma_{prol} < \gamma_c \ \& \ MI = 1 \\ \text{no proliferation} & \text{otherwise} \end{cases} \tag{23}$$

After mitosis process, one of the cells will occupy the position of the mother cell and the other will has a new position at a distance $2r$ from the mother cell, which can be calculated randomly as:

$$\begin{aligned} \mathbf{x}_{daut}^{(1)} &= \mathbf{x}_{moth} \\ \mathbf{x}_{daut}^{(2)} &= \mathbf{x}_{moth} + 2r\mathbf{e}_{rand}, \end{aligned} \tag{24}$$

where $\mathbf{x}_{moth}$ is the position vector of the progenitor cell, $\mathbf{x}_{daut}^{(1)}$ and $\mathbf{x}_{daut}^{(2)}$ are the position vector of the cells after the mitosis process and $\mathbf{e}_{rand}$ is a random unit vector.

Until the late 1990s, the belief that adult CM is unable to proliferate was widely defended. However, later studies presented contradictory evidences [86–88]. Nowadays, it is believed that adult CMs have, although low, some ability to proliferate (less than 1%) [88]. The ability to proliferate is closely related to the degree of CM differentiation through the cell-cycling arrest [72,89]. Recently, Roveimiab et al., on an interesting review of muscle cell migration, show the close relationship between the cell-cycling arrest and the mechanical conditions of the cell [90]. Concluding that it may be possible that cells re-enter the cell cycle by reducing cell junctions, which would result in a recovery of proliferation capacity. This restriction of the proliferation capacity with respect to the level of cell maturity has been taken into account in the present model. Thus, we consider that the CM goes through different degrees of cellular specialization reaching the maximum degree of specialization when establishing connections with other cells that cover at least half of the nodes of the cell membrane. At this stage, the cells reduce the capacity of proliferation to 1%.

2.4 Computational model

The model has been implemented within a user-defined subroutine (UELMAT [91]) within the commercial Finite Element (FE) software Abaqus Dassault Systems. A representative element is defined for the cells by a quasi-spherical element with 24 nodes that are representing the cell membrane (see Fig. 1). In this element, internal strains and stresses can be calculated as described in the previous sections. The cell is surrounded by a continuous medium (ECM) with which it interacts mechanically, evaluating the conditions of its environment and triggering the different cellular processes in response. The stresses transmitted by the cells, through the nodes located in the cell membrane, require a stress-strain balance inside the ECM. The interaction of the cell with the ECM generates deformations that require the solution of an elastic equilibrium problem of the entire ECM for every time step through the FE method. The ECM dimensions are $800x400x400\,\mu$m. It has been discretized by 128,000 trilinear hexahedral elements. The mechanical behavior of the ECM material has been considered as linear elastic. Boundary conditions have been described in Fig. 5. We consider free surfaces ECM and, to ensure calculation stability, points (1) and (2) are restricted in their planes. When external traction forces are applied on the $x = 0$ and $x = 800\,\mu$m planes, points (1) and (2) are maintaining the same restrictions. The algorithm of the model is detailed in Fig. 6. The proper-
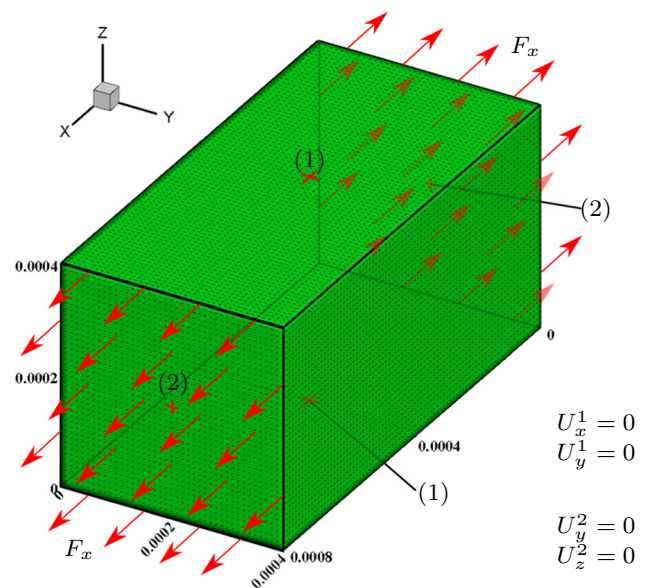

Fig. 5 Applied boundary conditions. To study the effect of ECM stiffness on cell fiber formation, a free surface ECM has been considered. In this case, for calculation issues, points (1) displacement in the direction of X and Y are restricted, while points (2) displacements in the directions Y and Z are restricted. To study the effect of external traction forces on cell alignment, homogeneous forces are applied on the planes $x = 0$ and $x = 800\,\mu$m combined with the previous restrictions of points (1) and (2). The value of applied force varies depending on the ECM stiffness and the desired level of deformation

ties and constants required for the calculation are listed in Tables 1 and 2.

3 Results

For the validation of the model, we developed a series of cases to compare their results with experimental cases from literature. The proposed cases aim is the study of the cellular response during the differentiation of MSCs in cardiac cells, as well as to study the effects of the mechanical conditions of the ECM on the systematic orientation of the cells. Cardiac tissue shows a high specialization in the generation of contractile stresses. They also show a preferred direction in which they are oriented and adhere to each other. This ability, common for the different types of muscle cells, is due to the reorientation and the growth of the cytoskeleton in well orientated structures. Likewise, the cells are able to join by means of stable junctions with which they are capable of transmitting stresses and electric potential. Several studies suggest an improvement of the mechanical properties developed by muscle tissues in-vitro via increasing cell alignment due to an increase in state of the cell maturation [15,92]. Therefore, we will simulate and study the effects of the application of different boundary conditions on the ECM in order to obtain
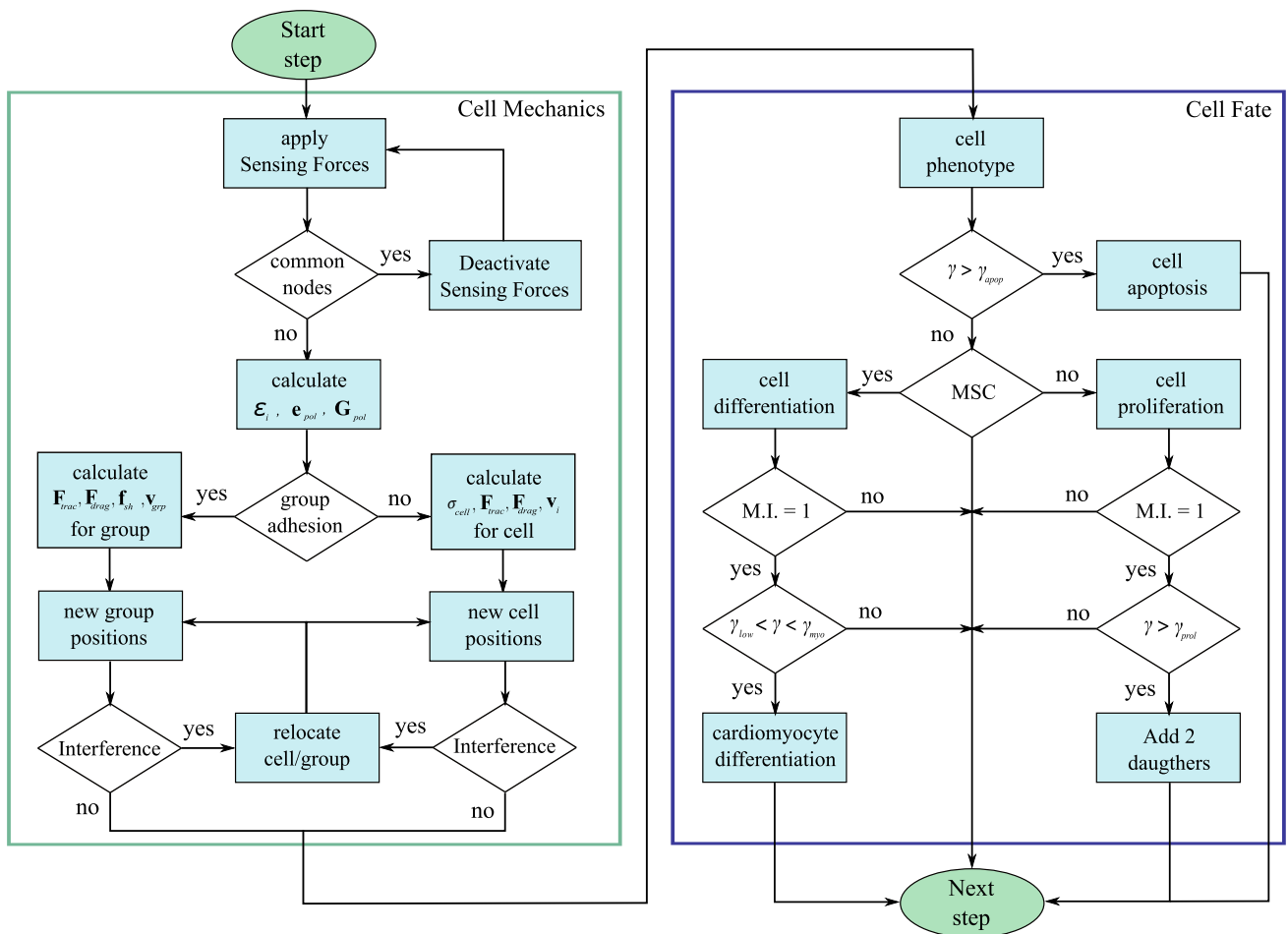
⌀ Springer

Fig. 6 Algorithm of the presented model for cell mechanics and cell fate. Cell differentiation, proliferation, apoptosis, and single and collective migration has been considered

Table 1 Mechanical parameters considered in the model

Parameter	Description	Value	References
K_{pas}	Stiffness of the cell passive elements	2.8 kPa	[51,52]
K_{act}^{msc}	Stiffness of the actin–myosin machinery of MSC	5.0 kPa	[51,52]
K_{act}^{cm}	Stiffness of the actin–myosin machinery of CM	7.0 kPa	[51,53,54]
ε_{max}	Maximum cell strain	0.09	[55–57]
ε_{min}	Minimum cell strain	-0.09	[55–57]
σ_{max}^{msc}	Maximum contractile stress exerted by the actin–myosin machinery on MSC	0.10 kPa	[58,59]
σ_{max}^{cm}	Maximum contractile stress exerted by the actin–myosin machinery on CM	0.25 kPa	[59,60]
ν	ECM Poisson ratio	0.4	[7,53]
η	ECM viscosity	1000 Pa s	[30,61]
k	Binding constant of the cell	10^8 mol^{-1}	[30,62,63]
n_{r_f}	Number of available receptors at the front of the cell	1.5×10^5	[64,65]
n_{r_b}	Number of available receptors at the back of the cell	1.0×10^5	[64,65]
ψ	Concentration of the ligands at the rear and the front of the cell	10^{-5} mol	[64,65]

Table 2 Defined thresholds to model cellular behavior

Parameter	Description	Value	References
l_{adh}	Minimum bound of projection to consider cell adhesion	0.50	[4,55]
γ_{low}	Lower bound of cell mechanical signal leading to CM differentiation	-0.04	[69,70]
γ_{myo}	Upper bound of cell mechanical signal leading to CM differentiation	-0.01	[69,70]
γ_{prol}	Maximum mechanical signal to cell proliferation	-0.20	[69,71]
γ_{apop}	Minimum mechanical signal leading to cell apoptosis	0.60	[55,71]
t_{min}	Minimum time needed for maturation	6 days	[9,72]
t_p	Time proportionality	200 days	[71,73,74]

the optimal stimulation conditions to improve the processes of tissue alignment and maturation.

3.1 Cell differentiation

In the last decades, the capacity of stem cells from different sources, multi and pluripotent, to express cardiac phenotype has been studied. As a result, it has been observed that the stiffness ranges of the ECM, which promote the expression of cardiac markers, can vary depending on the cellular source [93]. However, it is generally observed that these ranges are comparable to those that can be found in the heart tissue. Cardiac tissue is a tissue of intermediate stiffness whose stiffness varies between 10 and 20 kPa depending on the degree of maturity [7,69,94]. In this context, Li et al. [70], studied the effects of ECMs with a stiffness range between 16 and 65 kPa on MSCs differentiation. In these experiments, differentiation of CM was observed in ECMs whose rigidity was close to that of healthy tissue. Likewise, an improvement in the differentiation could be observed as the rigidity increases, ending by recommending stiffness close to 50 kPa. Later, Stoppel et al. [69], appointed that stiffness greater than those of healthy tissue could inhibit the correct maturation of cardiac cells. Besides, Young et al., 2014 have studied the difference between ECMs of 1, 11, and 34 kPa for CM culture. Their study showed that, although differentiation could be observed in ECMs of 34 kPa, whose rigidity was similar to that of fibrotic niches, the correct maturation of the cells could be affected by the high stiffness and this could have repercussions on the contractile capacities of the cells.

In the first studied case, differentiation of MSCs into CMs based on the ECM stiffness will be studied. A range of 8–20 kPa ECM stiffness has been chosen to employ. Initially, 40 MSCs were seeded randomly, in ECMs of 8, 10, 15, and 20 kPa, to study cellular differentiation during a period of 5 days, distributed in 200 steps. Each calculation step is equivalent to 0.6 h of cell–ECM interaction.

During the first hours, the cells dispersed throughout the ECM and migrate toward the center guided by the relative rigidity at the ECM center and the presence of other cells.

Once the center of the ECM is reached, the cells stay in that zone interacting with each other and forming cell clusters. After a certain time of interaction, for all cases, MSCs differentiate into CM. This differentiation takes place once the cell reaches a certain level of maturation. The time needed for this maturation depends on the level of the cell internal deformations, being greater on soft ECMs. Thus, the more rigid ECMs the faster the differentiation is. For instance, in ECM of 8.0 kPa, cells initiate the differentiation after 48 h, and after 92 h all the cells have been differentiated. In contrast, in ECM of 20.0 kPa, cells start the differentiation after 30 h, and after 60 h all the cells have been differentiated (Fig. 7).

ECM stiffness not only influences the differentiation process, but also the cell exerted forces. In Fig. 8, the average of cell traction forces is shown for the considered rigidities. It can be seen that in stiffer ECMs the traction forces are higher than in soft ECMs. Besides, in the curves, two transitions can be observed. The first one corresponds to the migration of the cells to the center zone, where their level of internal deformation falls and consequently it increases the traction forces. The second transition corresponds to cell differentiation. The phenotype change leads to a greater degree of specialization of the cells generating an increase in the average traction forces in this case.

3.2 Effect of ECM stiffness on cell fiber formation

In the second case study, the orientation and the formation of CM fibers in ECMs of 8, 10, 15, and 20 kPa are studied. Thereby, starting with differentiated CM, cell–cell and cell–ECM interactions are considered and simulated for 15 days. For each ECM stiffness, the experiment has been repeated 10 times. Random initial cell distributions have been generated for each repetition. The evaluation of the results has been made with the average of the results obtained from the 10 experiments for each stiffness. To contrast the obtained results, they have been compared with those obtained for fibroblasts in an ECM of 35 kPa, which is the appropriate stiffness for fibroblasts in cardiac fibrotic tissues [50,74].
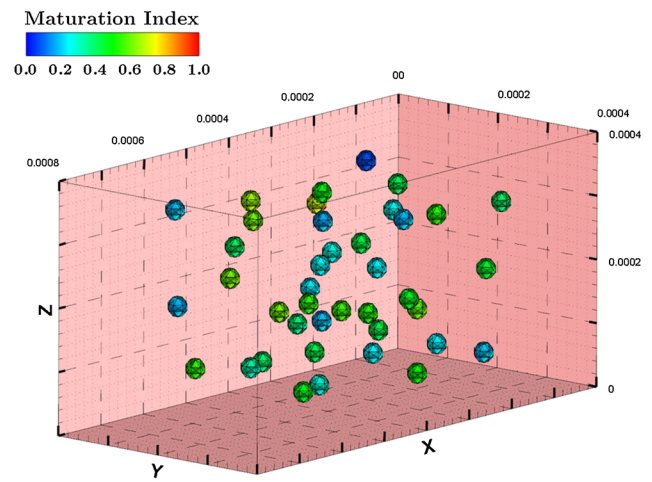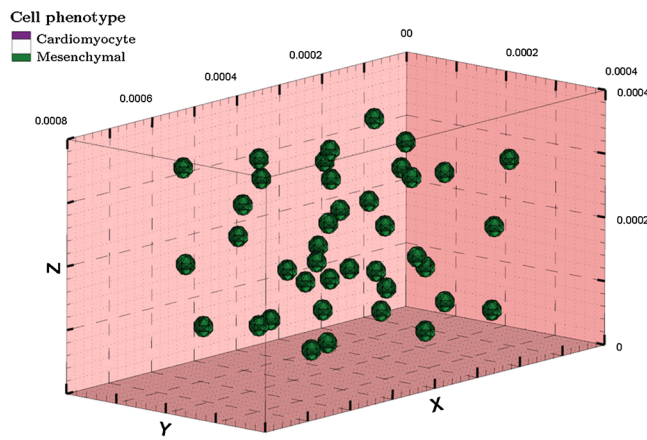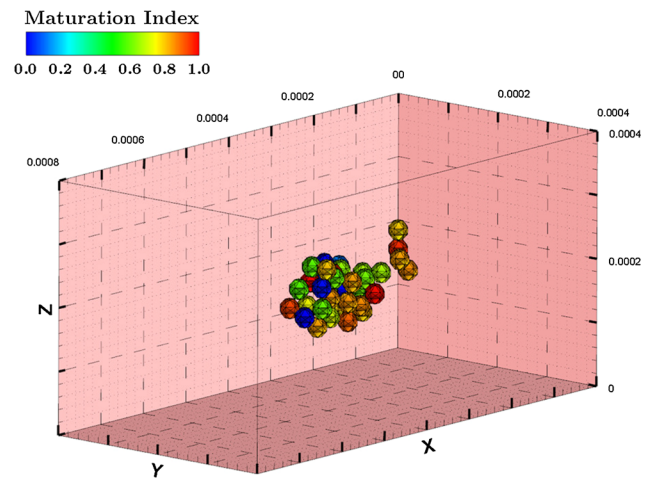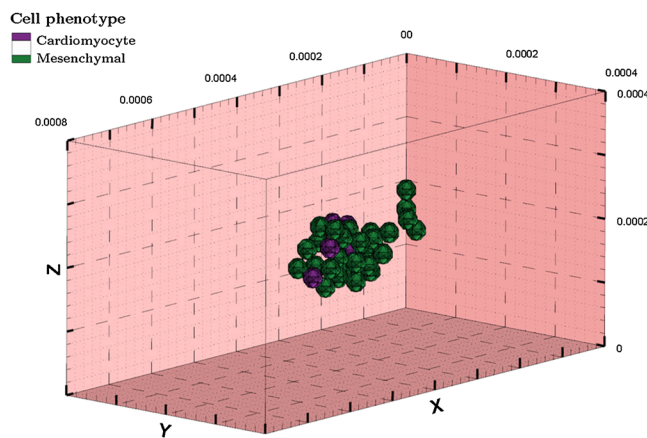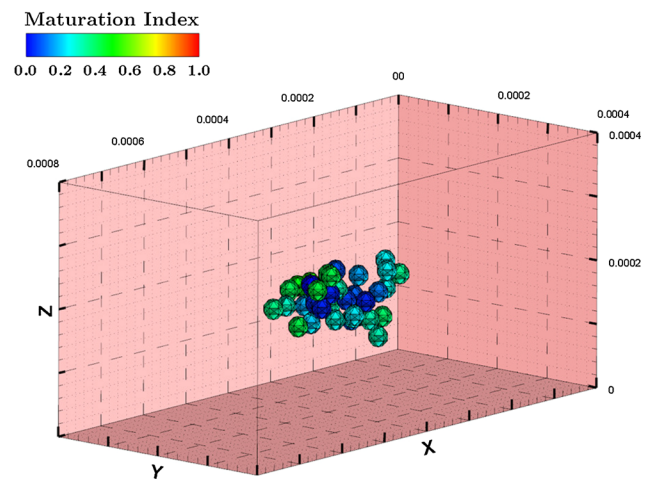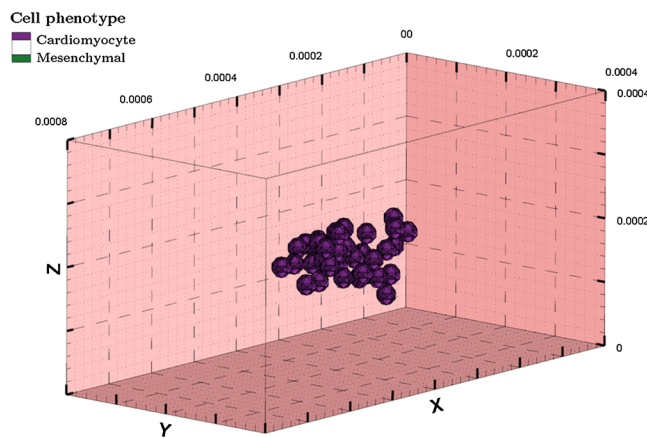
Fig. 7 Maturation state (right) and cell phenotype (left) (see also video Suppl_case_01). The cells are randomly distributed into a 20 kPa ECM. After 30 h in culture, the cells start to differentiate. After 60 h in culture, all the cells have differentiated into CM

After cell migration to the center of the ECM, the CM join to each other following the direction of $\mathbf{G}_{pol}$. In ECM of higher rigidity, this direction is closer to the longitudinal direction and elongated groups are formed. In contrast, fibroblasts form an aggregation with a spherical shape in

the ECM center (Fig. 9). Besides, increasing the stiffness improves cell maturation and proliferation rates, which explain the higher number of cells in stiffer ECMs. However, due to the low proliferation rate of CM in comparison
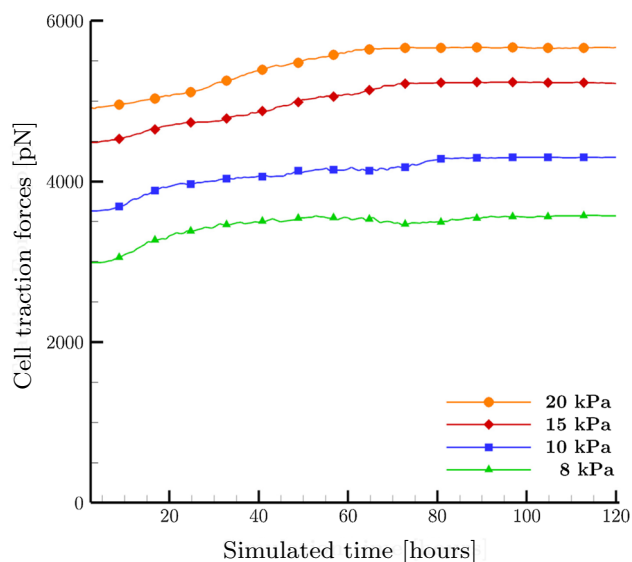
Fig. 8 Cell traction forces. Softer ECMs show higher traction forces than rigid ECMs. An increase in traction forces is observed after 70 h due to cell differentiation. The time necessary for cell differentiation is reduced by the ECM stiffness

with fibroblasts, the number of cells of the most rigid ECM is much lower than that achieved with fibroblasts [90].

It is also observed that, as the simulation progresses, the number of cells that are incorporated into the main chain (fiber) increases, obtaining, at the end of the simulation, the incorporation of almost the total of the cells in a single chain for all cases (Fig. 10a). We observed that, initially, the cells take longer time to join each other in softer ECMs, delaying chains formation, and increasing the variability of the results (Fig. 10b). At later time steps, we observe how both, the number of cells in the main chain and its elongated shape, are greater in stiffer ECMs [95–98]. After 15 days in culture, the groups formed in 8 kPa ECMs incorporate about 100 cells, while for 20 kPa ECMs, the groups formed incorporate 140 cells. Although the groups in the stiffest ECMs have a greater population, the appearance and alignment with respect to the longitudinal axis are, in general, better in stiffer ECMs.

To compare the shape of the fiber in the different cases, an aspect ratio, based on the groups' geometry, has been defined. The dimensionless parameter η_x, the aspect ratio, shows how the morphology of the group is geometrically correlated, and it is calculated as:

$$\eta_x = \left[\frac{L_x^2}{L_y L_z} \right]^{0.5}, \tag{25}$$

where L_x, L_y, and L_z, are the dimensions of the aggregation in X, Y and Z directions, respectively. In Fig. 10c an improvement in the aspect ratio can be observed as the stiffness of the ECM increases.

Along with the simulation, it can be seen that cell groups have the ability to move together [99]. Initially, small groups, made up of a few cells, have a movement capacity similar to that of individual cells. However, as the number of cells in the group grows, the movement of these groups slows down and even stops. Likewise, cells within the same group are able to relocate to new positions without leaving the group.

3.3 Mechanical stimuli (external traction force on ECM) on cell alignment

Mechanical stimuli (external traction force) can play a key role in adherent cell behavior. Cells such as CMs form anisotropic tissues in which there is a principal direction in which the forces are transmitted preferentially. These forces are transmitted from cell to cell through the cadherin-type junctions, which interconnect the cytoskeleton of the cells. The ability to transmit forces from one cell to another, as well as along the cell itself, depends on the degree of alignment of the cells with respect to the direction of that force. During embryonic development, a perfectly sequenced cascade of mechanical and chemical signals promote this alignment, stimulating the cells to generate functional muscle tissues [100]. The degree of functionality of tissues developed in-vitro depends on the ability to reproduce these stimuli. In recent years, a great effort has been exerted to develop different strategies to improve cell alignment in muscle tissues [15,69,101]. It has been possible to improve the degree of tissue maturation and contraction capacities. However, the generated forces by these in-vitro engineered muscle tissues are still lower than those observed in in-vivo tissues. In this way, understanding the close relationship between the mechanical conditions of the cell culture environment and the degree of cell alignment seems to be a key point to continue advancing towards the improvement of these in-vitro engineered tissues.

In the previous case, the effect of the ECM geometry has seemed to be decisive in cell alignment. In the present case study, a traction force has been applied to the ECM in the x-direction, achieving the deformation of the ECM in the range of 5–35%. Being a sustained permanent deformation, the cells have been considered to adapt their morphology to the deformed situation of the ECM. Thus, the passive deformations of the ECM are not considered when calculating the internal cell deformations. Moreover, due to this applied force, residual stresses have been generated in the ECM, which reduces the cell internal deformation in this direction, thus being able to influence the direction of the cell polarization.

To study this effect, a series of experiments on ECM with stiffness in the range of 8–50 kPa, have been generated. For each stiffness, traction forces have been applied in the x-direction equivalent to deformations in the range of 5–35%.
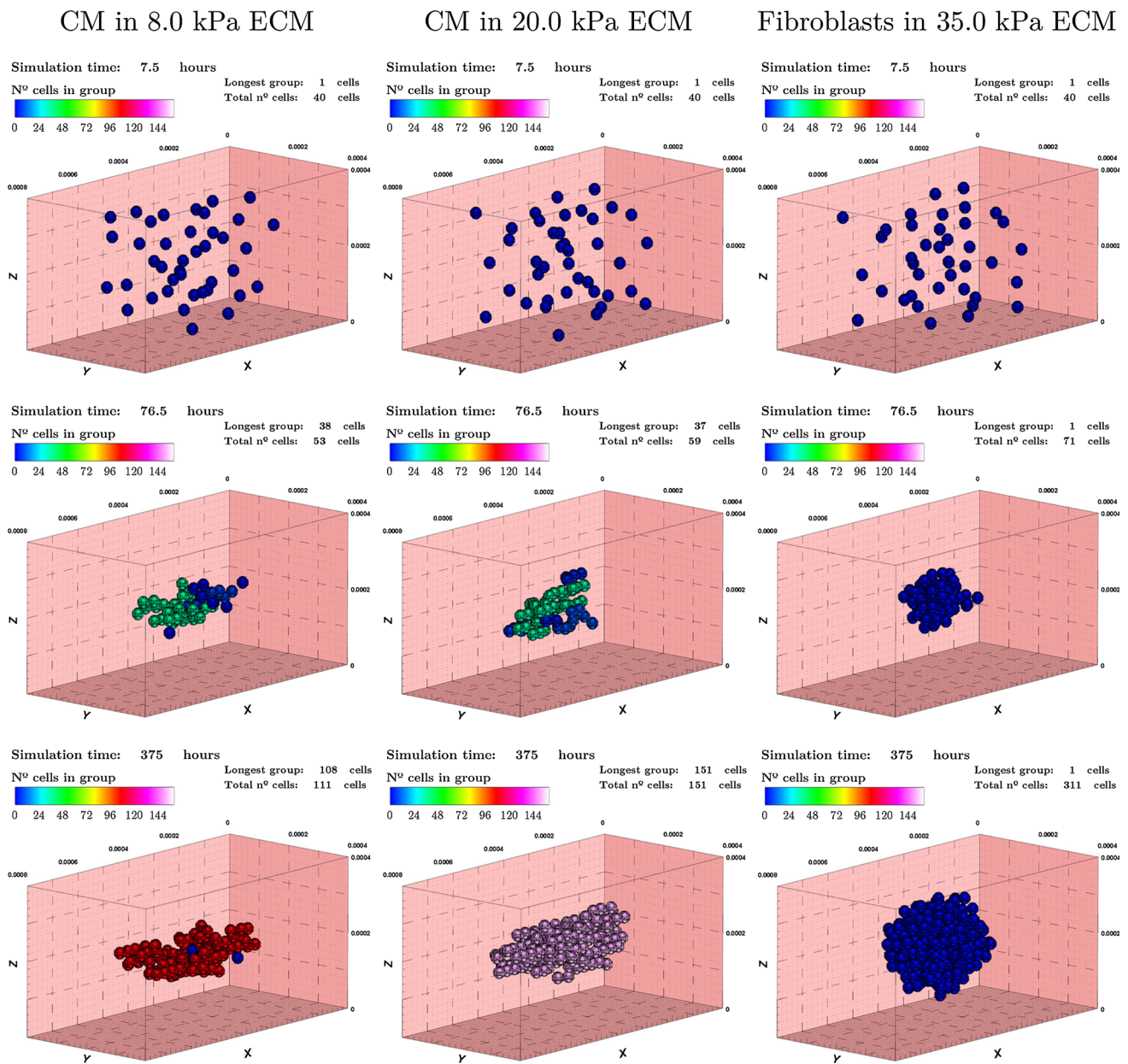
Fig. 9 CMs are seeded in ECMs of 8.0 and 20.0 kPa, and fibroblasts are seeded in 35.0 kPa ECM (see also video Suppl_case_02). Different morphologies are adopted by cell aggregations depending on the cell phenotype and ECM stiffness. CMs form groups along the direction of $\mathbf{G}_{pol}$, which is close to the longitudinal direction. In contrast, fibroblasts create spheroid aggregation in the ECM center

Each case has been repeated 10 times with initial random distributions of 40 cells.

In general, an improvement in the results with respect to the previous case can be observed (Fig. 11). The presence of internal stresses in the ECM, due to the effect of the applied force, reduces the internal cell deformations in the sensing phase, which translates into a faster maturation rate. As in the previous case, a greater number of cells are observed in stiffer ECMs. However, despite the increase in the rate of maturation, the proliferation does not seem to suffer a signif-

icant variation for 8 kPa ECMs. In general, in the main chain, an increase of the cell number is observed with the stiffness increase until a specific value (39 kPa) and then it decreases. Besides, as the applied traction force increases, the number of cells in the main group also increases until a specific value (20% of deformation) and then it decreases again (Fig. 12a). A reduction of the time necessary for the incorporation of 75 % of the cells in a single chain is observed in general until a specific value (29 kPa) and then it increases (Fig. 12b). Finally, an increase in the Aspect ratio can be observed until
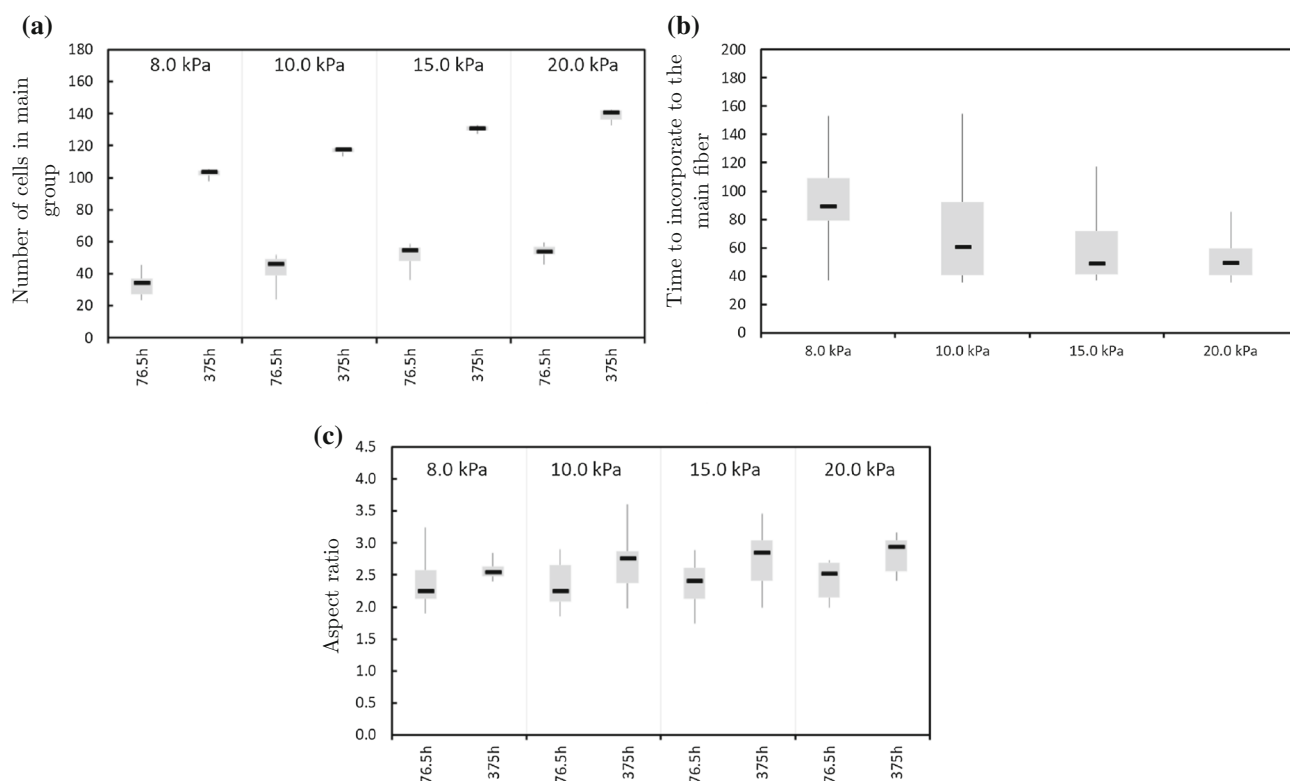
Fig. 10 Analysis of the effect of stiffness on chain (fiber) formation. **a** Number of cells that form the main group for 76.5 and 375 h. Stiffer ECMs show greater proliferation than soft ECMs and it also shows a higher number of cells in the main chain. **b** Time (hours) required for the incorporation of 75% of the cells in the main fiber in different ECM stiffness. As the stiffness increases, the time necessary for the cells to incorporate to the main chain drops. **c** Aspect ratio, the relationship between the length of the chain in the longitudinal and transverse direction for 76.5 and 375 h

a specific value (31 kPa) and then a slight decrease is observed (Fig. 12c).

These results are consistent with those obtained in different experimental works, where a cell alignment follows the direction of the imposed force or displacement [4,8,102–104].

4 Discussion

Cell migration depends on the interactions of cells with tissue structures, including ECM and other cells, establishing an interdependent evolution between them. Thus, cells respond to different stimuli (mechanical, electrical, thermal, and chemical) in different scales (subcellular, cellular, and multicellular) through ECM interactions, which influencing individual and/or collective migration processes. Mechanical properties of ECM are perhaps the most essential regulatory factor on cellular activity, being key in the regulation of processes such as migration, proliferation, differentiation, and apoptosis [105]. Due to the increasing interest in cell mechanics and cell mechanics modeling, several reviews can be found in the bibliography. Rorth [106] presented a com-

plete review of the different migration processes, as well as the influence of cell–cell interaction during collective migration, highlighting the role played by different cells in the group, which adopts specific cell phenotypes during collective migration. Later in 2016, Mayor et al. [107] presented a new review where they deepen into the process of collective migration with a special interest in cell–cell communication through molecular signaling which could be essential in the coordination of collective cell migration. In that same year, te Boekhorst et al. [108] presented another interesting review focused on the mechanical properties of the cell, such as the evolution of cell adhesions, or the deformations that appear in the cytoskeleton and the cell, during cell migration processes. They also add a good introduction to the developed computational models, as well as its interesting capabilities to bring new conclusions in this field. More recently van Helvert et al. [58], presented an updated review, where new concepts such as nano-topology and porosity, are presented with great interest in the analysis of cell mechanics. This review introduces a new approach in the consideration of cell–ECM interactions, being necessary to consider an active and reciprocal relationship between cells and ECM. Thus, the properties of the ECM could alter the cell properties, which
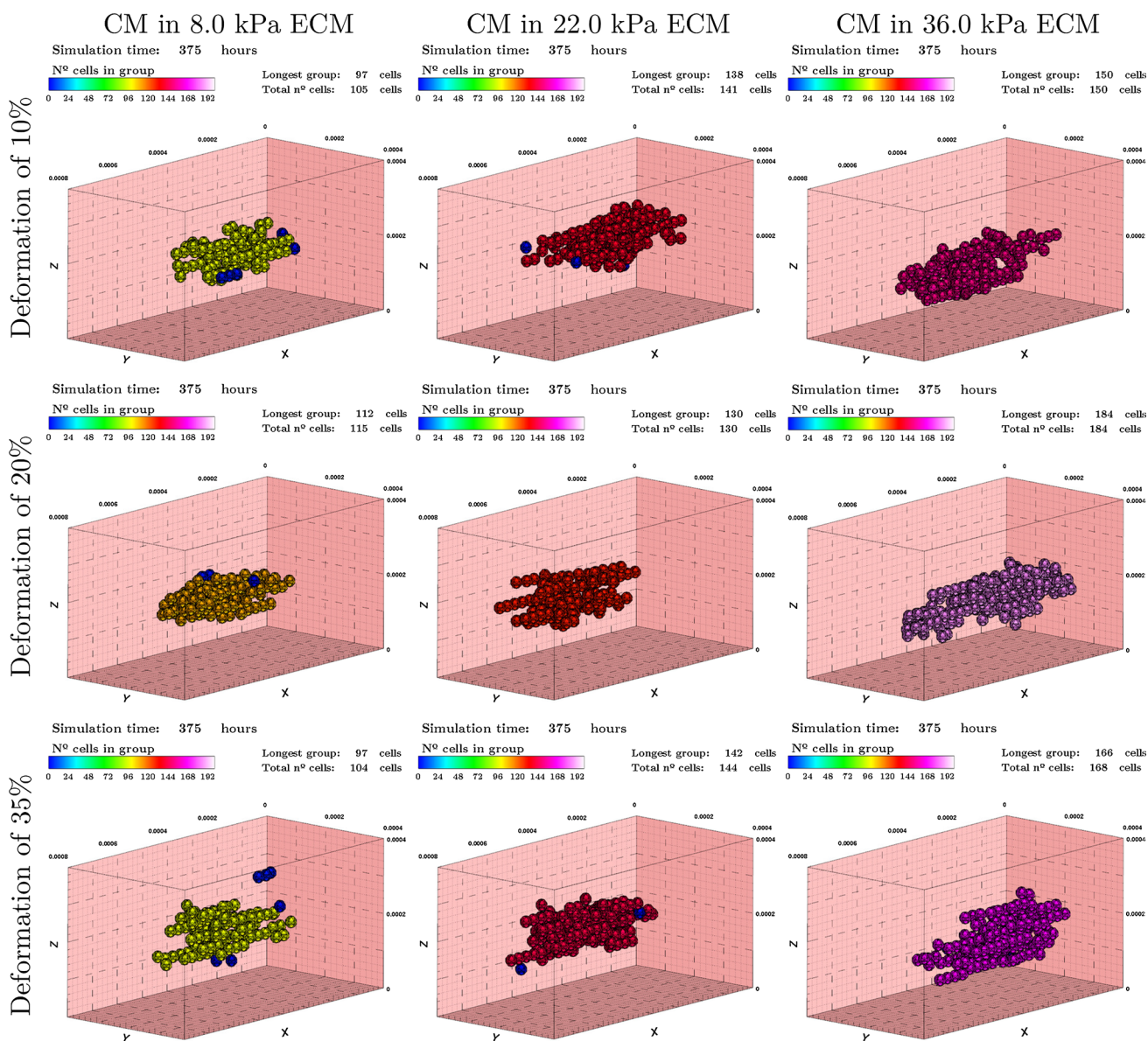
Fig. 11 CMs are seeded in ECMs of 8, 22, and 36 kPa after 15 days. Incremental traction values are applied in ascending order. (Top) Traction in *x*-direction equivalent to 10% of deformation (see also video Suppl_case_03(a) for ECMs of 36 kPa). (Middle) Traction in *x*-direction equivalent to 20% of deformation (see also video Suppl_case_03(b) for ECMs of 36 kPa). (Top) Traction in *x*-direction equivalent to 35% of deformation (see also video Suppl_case_03(c) for ECMs of 36 kPa). Better cell alignment and greater number of cells in the main group, can be observed as the stiffness increases. Better results were obtained in 36 kPa ECMs with 20% of deformation

in turn could modify the ECM, in a continuous process of reciprocal remodeling.

In the presented work, we purpose a 3D model to evaluate cell mechanics in complex mechanical ECMs with reciprocal interactions. This model has been applied to study cell differentiation, as well as cell–cell and cell–ECM interactions of cardiac cells, in the early stages of tissue formation, with a special interest in tissue architectures. To validate the model, a series of cases, based on experimental results from the literature, have been proposed.

In the first experiment, cell differentiation guided by substrate stiffness has been studied. The cell–ECM interaction generates internal cell deformations that are transcribed and transported to the cell nucleus, triggering specific genetic transcription protocols. After a time necessary for cell maturation, and which in turn is influenced by the ECM stiffness, the cells adopt cardiac-like phenotypes.

In the second experiment, cells migration is guided by both the mechanical stimuli generated by other cells and the geometry of the ECM. As the ECM has an elongated shape
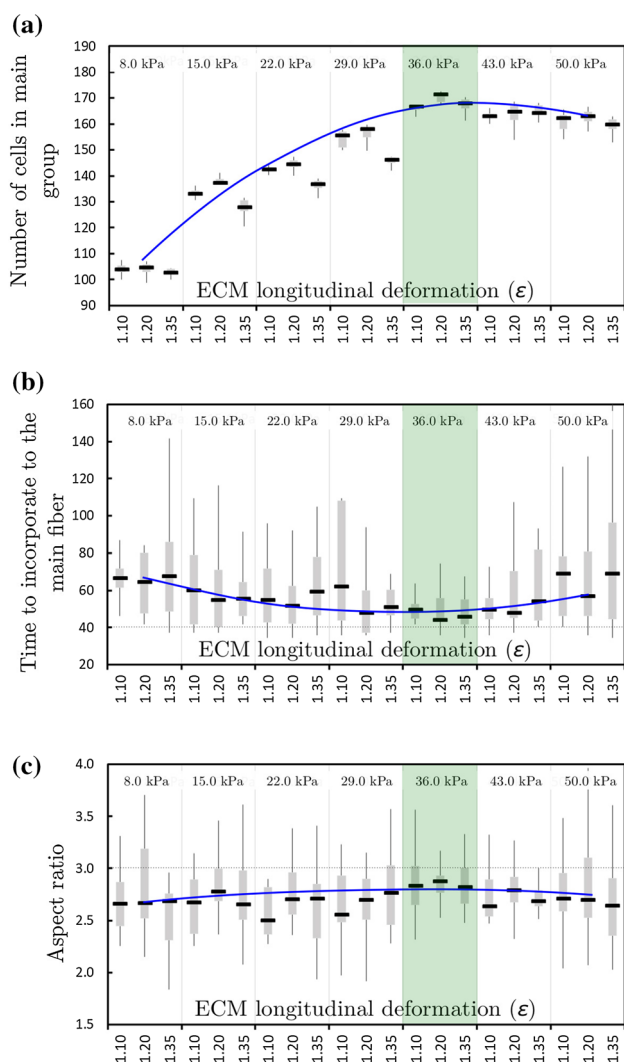
Fig. 12 The effect of the application of external traction forces in the formation of chains in ECMs with stiffness in the range of 8–50 kPa. Blue line represents the evolution of the results of the intermediate deformation ($\varepsilon = 1.20$) by a quadratic approximation. The optimum stiffness obtained from the quadratic approximation of the obtained results is between the values of 29 and 39 kPa (green band). **a** Number of cells that form the main chain after 15 days under deformations of 10, 20 and 35% of the ECM, respectively. An increase in the number of cells has been observed as the external traction force applied increases until a local maximum and then a decrease has been observed. **b** Time (hours) required for the incorporation of 75% of the cells in the main fiber after the application of different ECM strains. Minimum values, and less variability, have been obtained in 36 kPa ECMs stiffness. In general, the best results are observed for 20% of deformation. **c** Aspect ratio after 15 days. (Color figure online)

and the outer faces are free of constraints, the stiffness is relatively high in the longitudinal direction. Coupling of these two stimuli generates differences in the formation of groups for different stiffness. The effects of the neighboring cells are smaller in more rigid ECMs while the effect of the ECM geometry increases, being determinant for the quality of the formed chains. Initially, the effect of the stiffness in cell align-

ment does not seem conclusive. A slight improvement can be observed in the aspect ratio in Fig. 10c, with better results for the stiffest ECMs. Together with the number of cells that conform to the main chain, it is possible to conclude that larger chains, with equal or better morphology, can be obtained. Besides, as it evolves with the time, the aspect ratio and the size of the main chains increases in all cases. The incorporation of the cells to the main chain seems to be faster in stiffest ECMs. This is consistent with the well known cell behavior, that a cell migrates faster in stiffer ECMs. As the cells proliferate, the attraction force generated by cell clusters stimulates the cells to join rapidly the nearby groups. Due to the own morphology of the chain, there is a greater number of proliferating cells in the lateral cluster surface, which stimulate again the cellular growth to be higher in this direction than in the longitudinal one, reducing in this way the aspect ratio. Thereby, as a larger number of cells are incorporated into the main chain, a thickening effect of the chain can be observed.

In the third experiment, we observed longer and thinner chains. This improvement is reflected in the aspect ratio, where it is observed that it reaches values above 2.5 (Fig. 12c). However, it is also observed that an excessive ECM external applied traction force causes a drop in all the aspects. In 8 kPa ECMs, the time needed to incorporate 75% of the cells in the main chain, increases when the applied traction exceeds 2.0 kPa. However, an improvement with respect to the second experiment can be observed in all the cases for times below 90 h. In the 15 kPa ECM, a drop can be observed in both the number of cells in the main chain and in the aspect ratio. This is repeated for almost all the considered stiffness. All the cases have been exposed in a 3D graph in which the best quadratic fit plane is presented for global comparisons (Fig. 13). The number of cells seems to increase rapidly with the ECM stiffness (Fig. 13a). Furthermore, the time needed to incorporate 75% of the cells in the main group seems to decrease for intermediate stiffness (Fig. 13b). In comparison, results for AR seem to be correlated with the imposed deformation, with higher values in intermediate deformations (Fig. 13c). For all cases, these results seem to be related to the ECM deformation, showing worse results for strains above 25% and optimum results within the range of 20–25% of the ECM deformation (Fig. 13).

We observed local tendencies for each stiffness in function of the external imposed deformation, with better results for the intermediate deformations in almost all the cases. So, instead of using the full data set, for a better comparison of the results, we compare the obtained results for the intermediate deformation by obtaining the approximation curve that fits better to this data (see blue curve in Fig. 12). The order of the approximation curve was chosen based on the simplest approximation criterion but keeping a good fit with the obtained data. Thus, comparing quadratic, cubic, and quartic approaches, only slight differences could be found, conclud-

ing that the quadratic approximation curve was sufficient and adequate for this set of data. Considering this function, it can be concluded that the optimum stiffness range for obtaining aligned chains is between 29 and 39 kPa applying a mechanical stimulus equivalent to deformations of between 20 and 25%. This strain value is consistent with the working range of cardiac tissue [69]. The drop in higher strains may be caused by an excessive deformation which could hinder the interaction of the cell with the ECM. This effect could be equivalent to that is produced by a too rigid ECM, which complicates the cell penetration.

5 Conclusion

Here we present a 3D model for the analysis of CM behavior for tissue formation. So, a model of cell migration has been developed considering the formation of stable cell adhesions, and collective migration, depending on the mechanical stimuli of the cellular environment. Besides, the model includes the processes of differentiation, proliferation, and apoptosis, as a response to the mechanical conditions of the ECM. This model has been applied to study differentiation of MSCs into CMs, as well as their proliferation and the cellular architecture formation, due to the effect of the ECM mechanical properties. The results show a relationship between the geometry of the ECM and the generation of oriented fibers, as a consequence of the stiffness effects. These effects are increased by applying external loads that generate internal stresses in the ECM. The obtained results are qualitatively consistent with the bibliography [7,15,69,90,95–99,103].

The results show how the mechanical stimuli of the cell environment are essential for cell behavior, including differentiation, migration, proliferation, and apoptosis. For instance, MSCs in ECM in the range of embryonic heart stiffness trigger differentiation in CMs [69,70,109]. It is also observed how cells have a different response to different environment conditions, adopting different cellular architectures depending on the cell phenotype. Fibroblasts form a spherical aggregate of cells, while CMs adopt an elongated architecture, due to the tight junctions [105]. Besides, it can be observed how different mechanical stimulus impact on cell migration behavior. Initially, the cells feel differences in stiffness of the ECM and migrate accordingly. Once they reach a certain degree of closeness with other cells, the direction of migration varies, tending to get the cells closer together. We see that this effect depends strongly on the ECM stiffness, where the cells are able to feel each other at a greater distance in softer ECMs. While the cells are kept at a certain distance, the direction of majority polarization is given by the mechanical conditions of the medium. By applying an external traction load, it is possible to generate an influence in this direction of polarization, thereby achieving cells
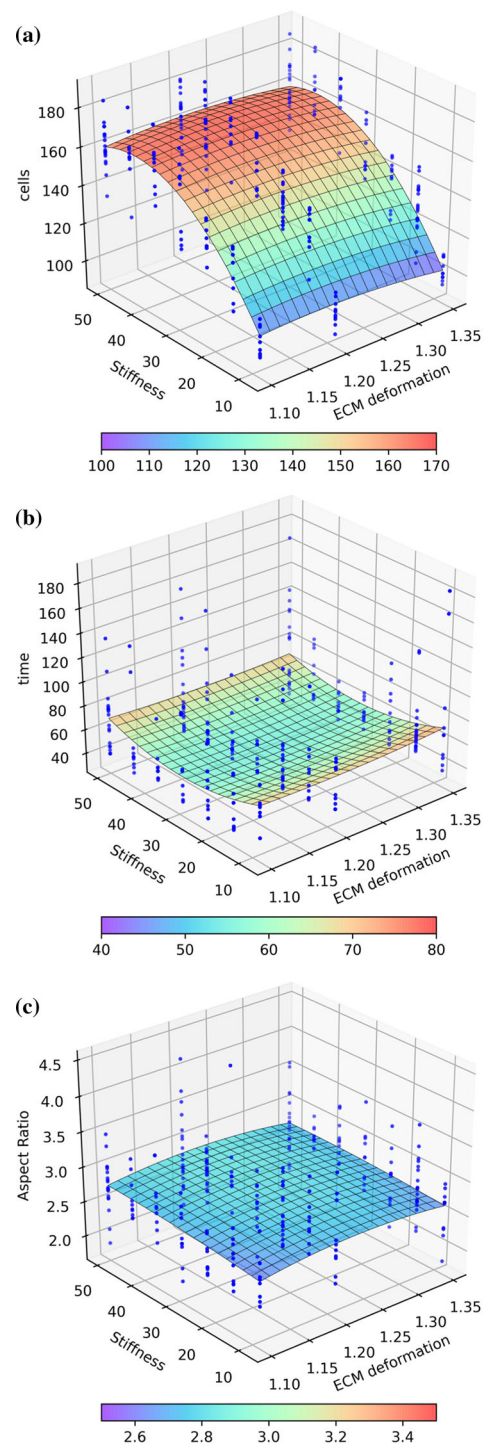

Fig. 13 The effect of the variation of the ECM stiffness and deformation with cell behavior. Better results are obtained for stiffness in the range of 30–40 kPa, and external deformations of 20%. **a** Number of cells increases rapidly with stiffness with less relevance of the imposed external force. **b** Groups are formed faster in intermediate stiffness. **c** Aspect ratio increases in the intermediate imposed deformations

alignment and adherence in a certain direction. Additionally, it is observed that the geometry of the ECM plays a key role, as well as the presence of external stimuli, such as the appli-

cation of external forces [4,103]. However, it is also noted that the application of excessive forces or excessive rigidity can have unfavorable consequences.

In summary, better results have been obtained for stiffer ECMs, where a higher proliferation rate is observed, due to faster maturation. Optimum results have been shown in ECMs with stiffness in the range of 29–39 kPa, applying a traction force in the x-direction equivalent to deformations in the range of 20–25%. However, softer ECMs, where cells are able to differentiate properly, could be beneficial initially. Thus, as proposed by Young et al. [74], it could be beneficial to work with materials whose stiffness could be adapted as the cells mature, achieving an ECM with a mechanical behavior closer to in-vivo tissue. Finally, as it has been demonstrated experimentally, applying external forces to stimulate mechanically the cells, improves both cell maturation and cell alignment, being able to obtain an anisotropic tissues oriented in a certain direction [4,103]. In this context, better results have been obtained applying ECM external deformations in the range of 20–25%, which is consistent with the deformations to which the cardiac tissue is subjected [69].

Cellular architecture plays a key role in the growth and development of tissue functionality [6,25]. This architecture is closely related to the presence of perfectly coordinated mechanical, thermal, chemical and electrical cues. The ability to understand and apply these stimuli in controlled environments will define the quality of tissues that can be developed in-vitro. The application of computational models that can easily reproduce complex environments, can present a great advantage when designing and analyzing experimental assays. With the present model, we want to take a step towards the understanding of these stimuli and offer a possible tool capable of optimizing the mechanical environments for cell cultures. Some simplifications and/or limitations have been considered in the proposed model, such as the consideration of constant cell morphology, and the consideration of the linear elastic behavior of the ECM. Some ECM characteristics such as topology, molecular networks, ECM remodeling, etc. should be taken into account. However, the presented model has the advantage of being simple, with a low computational cost and easy adjustment of the parameters for the study of different cases. In this way, even with these limitations, the present model can provide relevant information to deepen the study of cell migration and mechanobiology.

References

1. World Health Organization (2017) Cardiovascular diseases. http://www.who.int/es/news-room/fact-sheets/detail/cardiovascular-diseases- (cvds)

2. Ferrari R (2002) Healthy versus sick myocytes: metabolism, structure and function. Eur Heart J Suppl 4(G):G1–G12. https://doi.org/10.1016/S1520-765X(02)90084-2

3. Colvin M, Smith JM, Hadley N, Skeans MA, Carrico R, Uccellini K, Lehman R, Robinson A, Israni AK, Snyder JJ, Kasiske BL (2018) OPTN/SRTR 2016 annual data report: heart. Am J Transplant 18:291–362. https://doi.org/10.1111/ajt.14561

4. Costa KD, Lee EJ, Holmes JW (2003) Creating alignment and anisotropy in engineered heart tissue: role of boundary conditions in a model three-dimensional culture system. Tissue Eng 9(4):567–577. https://doi.org/10.1089/107632703768247278

5. Kim DH, Lipke EA, Kim P, Cheong R, Thompson S, Delannoy M, Suh KY, Tung L, Levchenko A (2010) Nanoscale cues regulate the structure and function of macroscopic cardiac tissue constructs. Proc Natl Acad Sci 107(2):565–570. https://doi.org/10.1073/pnas.0906504107

6. Bissell MJ, Rizki A, Mian IS (2003) Tissue architecture: the ultimate regulator of breast epithelial function. Curr Opin Cell Biol. https://doi.org/10.1016/j.ceb.2003.10.016

7. Bhana B, Iyer RK, Chen WLK, Zhao R, Sider KL, Likhitpanichkul M, Simmons CA, Radisic M (2010) Influence of substrate stiffness on the phenotype of heart cells. Biotechnol Bioeng 105(6):1148–1160. https://doi.org/10.1002/bit.22647

8. Mansour H, De Tombe PP, Samarel AM, Russell B (2004) Restoration of resting sarcomere length after uniaxial static strain is regulated by protein kinase Cϵ and focal adhesion kinase. Circ Res 94(5):642–649. https://doi.org/10.1161/01.RES.0000121101.32286.C8

9. Planat-Bénard V, Menard C, André M, Puceat M, Perez A, Garcia-Verdugo JM, Pénicaud L, Casteilla L (2004) Spontaneous cardiomyocyte differentiation from adipose tissue stroma cells. Circ Res 94(2):223–229. https://doi.org/10.1161/01.RES.0000109792.43271.47

10. Stedman HH, Sweeney HL, Shrager JB, Maguire HC, Panettieri RA, Petrof B, Narusawa M, Leferovich JM, Sladky JT, Kelly AM (1991) The mdx mouse diaphragm reproduces the degenerative changes of Duchenne muscular dystrophy. Nature 352(6335):536–539. https://doi.org/10.1038/352536a0

11. Heller LJ, Mohrman DE, Prohaska JR (2000) Decreased passive stiffness of cardiac myocytes and cardiac tissue from copper-deficient rat hearts. Am J Physiol Heart Circ Physiol 278(6):H1840–H1847

12. Madden L, Juhas M, Kraus WE, Truskey GA, Bursac N (2015) Bioengineered human myobundles mimic clinical responses of skeletal muscle to drugs. eLife. https://doi.org/10.7554/eLife.04885

13. Kim J, Oliveira VK, Yamamoto A, Perlingeiro RC (2017) Generation of skeletal myogenic progenitors from human pluripotent stem cells using non-viral delivery of minicircle DNA. Stem Cell Res 23:87–94. https://doi.org/10.1016/j.scr.2017.07.013

14. Ye L, Zhang S, Greder L, Dutton J, Keirstead SA, Lepley M, Zhang L, Kaufman D, Zhang J (2013) Effective cardiac myocyte differentiation of human induced pluripotent stem cells requires VEGF. PLoS ONE 8(1):201–205. https://doi.org/10.1371/journal.pone.0053764

15. Zhang D, Shadrin IY, Lam J, Xian HQ, Snodgrass HR, Bursac N (2013) Tissue-engineered cardiac patch for advanced functional maturation of human ESC-derived cardiomyocytes. Biomaterials 34(23):5813–5820. https://doi.org/10.1016/j.biomaterials.2013.04.026

16. Jackman CP, Ganapathi AM, Asfour H, Qian Y, Allen BW, Li Y, Bursac N (2018) Engineered cardiac tissue patch maintains structural and electrical properties after epicardial implantation. Biomaterials 159:48–58. https://doi.org/10.1016/j.biomaterials.2018.01.002

17. Yang G, Xiao Z, Ren X, Long H, Ma K, Qian H, Guo Y (2017) Obtaining spontaneously beating cardiomyocyte-like cells from adipose-derived stromal vascular fractions cultured on enzyme-crosslinked gelatin hydrogels. Sci Rep 7(February):1–11. https://doi.org/10.1038/srep41781

18. Jackman CP, Carlson AL, Bursac N (2016) Dynamic culture yields engineered myocardium with near-adult functional output. Biomaterials 111:66–79. https://doi.org/10.1016/j.biomaterials.2016.09.024

19. Rao L, Qian Y, Khodabukus A, Ribar T, Bursac N (2018) Engineering human pluripotent stem cells into a functional skeletal muscle tissue. Nat Commun 9(1):126. https://doi.org/10.1038/s41467-017-02636-4

20. Carlier A, Skvortsov GA, Hafezi F, Ferraris E, Patterson J, Koc B, Van Oosterwyck H (2016) Computational model-informed design and bioprinting of cell-patterned constructs for bone tissue engineering. Biofabrication 8(2):025009. https://doi.org/10.1088/1758-5090/8/2/025009

21. Galbusera F, Cioffi M, Raimondi MT (2008) An in silico bioreactor for simulating laboratory experiments in tissue engineering. Biomed Microdevices 10(4):547–554. https://doi.org/10.1007/s10544-008-9164-9

22. Galbusera F, Cioffi M, Raimondi MT, Pietrabissa R (2007) Computational modeling of combined cell population dynamics and oxygen transport in engineered tissue subject to interstitial perfusion. Comput Methods Biomech Biomed Eng 10(4):279–287. https://doi.org/10.1080/10255840701318404

23. Khayyeri H, Checa S, Tägil M, O'Brien FJ, Prendergast PJ (2010) Tissue differentiation in an in vivo bioreactor: in silico investigations of scaffold stiffness. J Mater Sci Mater Med 21(8):2331–2336. https://doi.org/10.1007/s10856-009-3973-0

24. Sandino C, Planell JA, Lacroix D (2008) A finite element study of mechanical stimuli in scaffolds for bone tissue engineering. J Biomech 41(5):1005–1014. https://doi.org/10.1016/j.jbiomech.2007.12.011

25. Gumbiner BM (1996) Cell adhesion: the molecular basis of tissue architecture and morphogenesis. Cell 84(3):345–357. https://doi.org/10.1016/S0092-8674(00)81279-9

26. Griffith LG (2002) Tissue engineering-current challenges and expanding opportunities. Science 295(5557):1009–1014. https://doi.org/10.1126/science.1069210

27. Pampaloni F, Reynaud EG, Stelzer EHK (2007) The third dimension bridges the gap between cell culture and live tissue. Mol Cell Biol 8(october):839–845

28. Giannitelli SM, Accoto D, Trombetta M, Rainer A (2014) Current trends in the design of scaffolds for computer-aided tissue engineering. Acta Biomater. https://doi.org/10.1016/j.actbio.2013.10.024

29. Ramtani S (2004) Mechanical modelling of cell/ECM and cell/cell interactions during the contraction of a fibroblast-populated collagen microsphere: theory and model simulation. J Biomech 37(11):1709–1718. https://doi.org/10.1016/j.jbiomech.2004.01.028

30. Zaman MH, Kamm RD, Matsudaira P, Lauffenburger DA (2005) Computational model for cell migration in three-dimensional matrices. Biophys J 89(2):1389–1397. https://doi.org/10.1529/biophysj.105.060723

31. Mogilner A (2009) Mathematics of cell motility: have we got its number? J Math Biol 58(1–2):105–134. https://doi.org/10.1007/s00285-008-0182-2

32. Mousavi SJ, Doweidar M, Doblaré M (2014) Computational modelling and analysis of mechanical conditions on cell locomotion and cell–cell interaction. Comput Methods Biomech Biomed Eng 17(6):678–693. https://doi.org/10.1080/10255842.2012.710841

33. Stéphanou A, Mylona E, Chaplain M, Tracqui P (2008) A computational model of cell migration coupling the growth of focal adhesions with oscillatory cell protrusions. J Theor Biol 253(4):701–716. https://doi.org/10.1016/j.jtbi.2008.04.035

34. Marzban B, Yuan H (2017) The effect of thermal fluctuation on the receptor-mediated adhesion of a cell membrane to an elastic substrate. Membranes 7(2):24. https://doi.org/10.3390/membranes7020024

35. Göktepe S, Abilez OJ, Parker KK, Kuhl E (2010) A multiscale model for eccentric and concentric cardiac growth through sarcomerogenesis. J Theor Biol 265(3):433. https://doi.org/10.1016/j.jtbi.2010.04.023

36. Shao D, Rappel WJ, Levine H (2010) Computational model for cell morphodynamics. Phys Rev Lett 105(10):108104. https://doi.org/10.1103/PhysRevLett.105.108104

37. Mousavi SJ, Doblaré M, Doweidar MH (2014) Computational modelling of multi-cell migration in a multi-signalling substrate. Phys Biol 11(2):026002. https://doi.org/10.1088/1478-3975/11/2/026002

38. Mousavi SJ, Doweidar MH (2014) A novel mechanotactic 3D modeling of cell morphology. Phys Biol 11(4):046005. https://doi.org/10.1088/1478-3975/11/4/046005

39. Mousavi SJ, Doweidar MH (2015) Role of mechanical cues in cell differentiation and proliferation: a 3D numerical model. PLoS ONE 10(5):e0124529. https://doi.org/10.1371/journal.pone.0124529

40. Mogilner A, Oster G (1996) Cell motility driven by actin polymerization. Biophys J 71(6):3030. https://doi.org/10.1016/S0006-3495(96)79496-1

41. Gavagnin E, Yates CA (2018) In: Handbook of statistics, vol 39 pp 37–91. https://doi.org/10.1016/bs.host.2018.06.002

42. Higazi AA, Kniss D, Manuppello J, Barnathan ES, Cines DB (1996) Thermotaxis of human trophoblastic cells. Placenta 17(8):683. https://doi.org/10.1016/S0143-4004(96)80019-1

43. Discher DE (2005) Tissue cells feel and respon to the stiffness of their substrate. Science 310(5751):1139–1143. https://doi.org/10.1126/science.1116995

44. Zhao M (2009) Electrical fields in wound healing: an overriding signal that directs cell migration. Semin Cell Dev Biol 20(6):674–687. https://doi.org/10.1016/j.semcdb.2008.12.009

45. Lintz M, Muñoz A, Reinhart-King CA (2017) The mechanics of single cell and collective migration of tumor cells. J Biomech Eng 139(2):021005. https://doi.org/10.1115/1.4035121

46. Ridley AJ, Schwartz MA, Burridge K, Firtel RA, Ginsberg MH, Borisy G, Parsons JT, Horwitz AR (2003) Cell migration: integrating signals from front to back. Science. https://doi.org/10.1126/science.1092053

47. Huh D, Hamilton GA, Ingber DE (2011) From 3D cell culture to organs-on-chips. Trends Cell Biol 21(12):745–754. https://doi.org/10.1016/J.TCB.2011.09.005

48. Brandi ML (2009) Microarchitecture, the key to bone quality. Rheumatology 48:iv3–iv8. https://doi.org/10.1093/rheumatology/kep273

49. Mousavi SJ (2015) Computational modeling of cell behavior in three-dimensional matrices. Ph.D. thesis, Universidad de Zaragoza

50. Mousavi SJ, Doweidar MH, Doblaré M (2013) 3D computational modelling of cell migration: a mechano-chemo-thermo-electrotaxis approach. J Theor Biol 329:64–73. https://doi.org/10.1016/j.jtbi.2013.03.021

51. Schäfer A, Radmacher M (2005) Influence of myosin II activity on stiffness of fibroblast cells. Acta Biomater 1(3):273–280. https://doi.org/10.1016/j.actbio.2005.02.004

52. Darling EM, Topel M, Zauscher S, Vail TP, Guilak F (2008) Viscoelastic properties of human mesenchymally-derived stem cells and primary osteoblasts, chondrocytes, and adipocytes. J Biomech 41(2):454–464. https://doi.org/10.1016/j.jbiomech.2007.06.019

53. Mathur AB, Collinsworth AM, Reichert WM, Kraus WE, Truskey GA (2001) Endothelial, cardiac muscle and skeletal muscle exhibit different viscous and elastic properties as determined by atomic force microscopy. J Biomech 34(12):1545–1553. https://doi.org/10.1016/S0021-9290(01)00149-X

54. Shi X, Qin L, Zhang X, He K, Xiong C, Fang J, Fang X, Zhang Y (2011) Elasticity of cardiac cells on the polymer substrates with different stiffness: an atomic force microscopy study. Phys Chem Chem Phys 13(16):7540. https://doi.org/10.1039/c1cp20154a

55. Chen QZ, Harding SE, Ali NN, Lyon AR, Boccaccini AR (2008) Biomaterials in cardiac tissue engineering: ten years of research survey. Mater Sci Eng R Rep 59(1–6):1–37. https://doi.org/10.1016/j.mser.2007.08.001

56. Roy P, Petroll W, Cavanagh H, Chuong C, Jester J (1997) An in vitro force measurement assay to study the early mechanical interaction between corneal fibroblasts and collagen matrix. Exp Cell Res 232(1):106–117. https://doi.org/10.1006/excr.1997.3511

57. Koch TM, Münster S, Bonakdar N, Butler JP, Fabry B (2012) 3D traction forces in cancer cell invasion. PLoS ONE 7(3):e33476. https://doi.org/10.1371/journal.pone.0033476

58. van Helvert S, Storm C, Friedl P (2018) Mechanoreciprocity in cell migration. Nat Cell Biol 20(1):8–20. https://doi.org/10.1038/s41556-017-0012-0

59. Gardel ML, Sabass B, Ji L, Danuser G, Schwarz US, Waterman CM (2008) Traction stress in focal adhesions correlates biphasically with actin retrograde flow speed. J Cell Biol 183(6):999–1005. https://doi.org/10.1083/jcb.200810060

60. Rodriguez ML, Graham BT, Pabon LM, Han SJ, Murry CE, Sniadecki NJ, Pabon LM, Murry CE, Graham BT, Han SJ, Rodriguez ML, Graham BT, Pabon LM, Han SJ, Murry CE, Sniadecki NJ, Pabon LM, Murry CE, Graham BT, Han SJ, Rodriguez ML (2014) Measuring the contractile forces of human induced pluripotent stem cell-derived cardiomyocytes with arrays of microposts. J Biomech Eng 136(5):051005. https://doi.org/10.1115/1.4027145

61. Duan B, Kapetanovic E, Hockaday L, Butcher J (2014) Three-dimensional printed trileaflet valve conduits using biological hydrogels and human valve interstitial cells. Acta Biomater 10(5):1836–1846. https://doi.org/10.1016/j.actbio.2013.12.005

62. Akiyama SK, Yamada KM (1985) The interaction of plasma fibronectin with fibroblastic cells in suspension. J Biol Chem 260(7):4492–4500

63. Akiyama SK, Hasegawa E, Hasegawa T, Yamada KM (1985) The interaction of fibronectin fragments with fibroblastic cells. J Biol Chem 260(24):13256–13260

64. Berry H, Larreta-Garde V (1999) Oscillatory behavior of a simple kinetic model for proteolysis during cell invasion. Biophys J 77(2):655–665. https://doi.org/10.1016/S0006-3495(99)76921-3

65. Mousavi SJ, Doweidar MH (2018) Encapsulated piezoelectric nanoparticle-hydrogel smart material to remotely regulate cell differentiation and proliferation: a finite element model. Comput. Mech. https://doi.org/10.1007/s00466-018-1604-7

66. Aragona M, Panciera T, Manfrin A, Giulitti S, Michielin F, Elvassore N, Dupont S, Piccolo S (2013) A mechanical checkpoint controls multicellular growth through YAP/TAZ regulation by actin-processing factors. Cell 154(5):1047–1059. https://doi.org/10.1016/j.cell.2013.07.042

67. Low BC, Pan CQ, Shivashankar GV, Bershadsky A, Sudol M, Sheetz M (2014) YAP/TAZ as mechanosensors and mechanotransducers in regulating organ size and tumor growth. FEBS Lett. 588(16):2663–2670. https://doi.org/10.1016/j.febslet.2014.04.012

68. Abercrombie M (1979) Contact inhibition and malignancy. Nature 281(5729):259–262. https://doi.org/10.1038/281259a0

69. Stoppel WL, Kaplan DL, Black LD (2016) Electrical and mechanical stimulation of cardiac cells and tissue constructs. Adv. Drug Deliv. Rev. 96:135–155. https://doi.org/10.1016/j.addr.2015.07.009

70. Li Z, Guo X, Palmer AF, Das H, Guan J (2012) High-efficiency matrix modulus-induced cardiac differentiation of human mesenchymal stem cells inside a thermosensitive hydrogel. Acta Biomater. 8(10):3586–3595. https://doi.org/10.1016/j.actbio.2012.06.024

71. Kang Kt, Park Jh, Kim Hj, Lee HyHm, Lee Ki, Jung Hh, Lee HyHm, Jang JW (2011) Study of tissue differentiation of mesenchymal stem cells by mechanical stimuli and an algorithm for bone fracture healing. Tissue Eng Regen Med 8(4):359–370

72. Asumda FZ, Asumda FZ (2013) Towards the development of a reliable protocol for mesenchymal stem cell cardiomyogenesis. Stem Cell Discov 03(01):13–21. https://doi.org/10.4236/scd.2013.31003

73. Wu QQ, Chen Q (2000) Mechanoregulation of chondrocyte proliferation, maturation, and hypertrophy: ion-channel dependent transduction of matrix deformation signals. Exp Cell Res 256(2):383–391. https://doi.org/10.1006/excr.2000.4847

74. Young JL, Kretchmer K, Ondeck MG, Zambon AC, Engler AJ (2015) Mechanosensitive kinases regulate stiffness-induced cardiomyocyte maturation. Sci Rep 4(1):6425. https://doi.org/10.1038/srep06425

75. Engler AJ, Sen S, Sweeney HL, Discher DE (2006) Matrix elasticity directs stem cell lineage specification. Cell 126(4):677–689. https://doi.org/10.1016/j.cell.2006.06.044

76. Huebsch N, Arany PR, Mao AS, Shvartsman D, Ali OA, Bencherif SA, Rivera-Feliciano J, Mooney DJ (2010) Harnessing traction-mediated manipulation of the cell/matrix interface to control stem-cell fate. Nat Mater 9(6):518–526. https://doi.org/10.1038/nmat2732

77. Kearney EM, Prendergast PJ, Campbell Va (2008) Mechanisms of strain-mediated mesenchymal stem cell apoptosis. J Biomech Eng 130(6):061004. https://doi.org/10.1115/1.2979870

78. Elmore S (2007) Apoptosis: a review of programmed cell death. Toxicol Pathol 35(4):495–516. https://doi.org/10.1080/01926230701320337

79. Trubelja A, Bao G (2018) Molecular mechanisms of mechanosensing and mechanotransduction in living cells. Extreme Mech Lett 20:91–98. https://doi.org/10.1016/j.eml.2018.01.011

80. Buxboim A, Ivanovska IL, Discher DE (2010) Matrix elasticity, cytoskeletal forces and physics of the nucleus: how deeply do cells 'feel' outside and in? J Cell Sci 123(3):297–308. https://doi.org/10.1242/jcs.041186

81. Delaine-Smith RM, Reilly GC (2012) Mesenchymal stem cell responses to mechanical stimuli. Muscles Ligaments Tendons J 2(3):169–180

82. Ulrich TA, De Juan Pardo EM, Kumar S (2009) The mechanical rigidity of the extracellular matrix regulates the structure, motility, and proliferation of glioma cells. Cancer Res 69(10):4167–4174. https://doi.org/10.1158/0008-5472.CAN-08-4859

83. Fouliard S, Benhamida S, Lenuzza N, Xavier F (2009) Modeling and simulation of cell populations interaction. Math Comput Model 49(11–12):2104–2108. https://doi.org/10.1016/j.mcm.2008.07.003

84. Hatzistergos KE, Quevedo H, Oskouei BN, Hu Q, Feigenbaum GS, Margitich IS, Mazhari R, Boyle AJ, Zambrano JP, Rodriguez JE, Dulce R, Pattany PM, Valdes D, Revilla C, Held-

man AW, McNiece I, Hare JM (2010) Bone marrow mesenchymal stem cells stimulate cardiac stem cell proliferation and differentiation. Circ Res 107(7):913–922. https://doi.org/10.1161/CIRCRESAHA.110.222703

85. Cheng G, Tse J, Jain RK, Munn LL (2009) Micro-environmental mechanical stress controls tumor spheroid size and morphology by suppressing proliferation and inducing apoptosis in cancer cells. PLoS ONE 4(2):e4632. https://doi.org/10.1371/journal.pone.0004632

86. Foglia MJ, Poss KD (2016) Building and re-building the heart by cardiomyocyte proliferation. Development 143(5):729–740. https://doi.org/10.1242/dev.132910

87. Vargas-González A (2014) La proliferación de los miocitos ventriculares del corazón de mamífero adulto: un fenómeno esporádico pero factible. Archiv Cardiología de México 84(2):102–109. https://doi.org/10.1016/j.acmx.2014.01.002

88. Yutzey KE (2017) Cardiomyocyte proliferation. Circ Res 120(4):627–629. https://doi.org/10.1161/circresaha.116.310058

89. Ahuja P, Sdek P, MacLellan WR (2007) Cardiac myocyte cell cycle control in development, disease, and regeneration. Physiol Rev 87(2):521–544. https://doi.org/10.1152/physrev.00032.2006

90. Roveimiab Z, Lin F, Anderson JE (2019) Emerging development of microfluidics-based approaches to improve studies of muscle cell migration. Tissue Eng Part B Rev 25(1):30–45. https://doi.org/10.1089/ten.teb.2018.0181

91. Abaqus 6.11 User Subroutines Reference Manual (2011)

92. Bian W, Bursac N (2009) Engineered skeletal muscle tissue networks with controllable architecture. Biomaterials 30(7):1401–1412. https://doi.org/10.1016/j.biomaterials.2008.11.015

93. Sheehy SP, Grosberg A, Parker KK (2012) The contribution of cellular mechanotransduction to cardiomyocyte form and function. Biomech Model Mechanobiol 11(8):1227–1239. https://doi.org/10.1007/s10237-012-0419-2

94. Chen QZZ, Bismarck A, Hansen U, Junaid S, Tran MQ, Harding SE, Ali NN, Boccaccini AR (2008) Characterisation of a soft elastomer poly(glycerol sebacate) designed to match the mechanical properties of myocardial tissue. Biomaterials 29(1):47–57. https://doi.org/10.1016/j.biomaterials.2007.09.010

95. Ye J, Boyle AJ, Shih H, Sievers RE, Wang ZE, Gormley M, Yeghiazarians Y (2013) CD45-positive cells are not an essential component in cardiosphere formation. Cell Tissue Res 351(1):201–205. https://doi.org/10.1007/s00441-012-1511-8

96. Ikonen L, Kerkelä E, Metselaar G, Stuart MCA, de Jong MR, Aalto-Setälä K (2013) 2D and 3D self-assembling nanofiber hydrogels for cardiomyocyte culture. BioMed Res Int 2013:1–12. https://doi.org/10.1155/2013/285678

97. Formigli L, Francini F, Nistri S, Margheri M, Luciani G, Naro F, Silvertown JD, Orlandini SZ, Meacci E, Bani D (2009) Skeletal myoblasts overexpressing relaxin improve differentiation and communication of primary murine cardiomyocyte cell cultures. J Mol Cell Cardiol 47(2):335–345. https://doi.org/10.1016/j.yjmcc.2009.05.008

98. Sassoli C, Pini A, Mazzanti B, Quercioli F, Nistri S, Saccardi R, Orlandini SZ, Bani D, Formigli L (2011) Mesenchymal stromal cells affect cardiomyocyte growth through juxtacrine Notch-1/Jagged-1 signaling and paracrine mechanisms: Clues for cardiac regeneration. J Mol Cell Cardiol 51(3):399–408. https://doi.org/10.1016/j.yjmcc.2011.06.004

99. Tahara N, Brush M, Kawakami Y (2016) Cell migration during heart regeneration in zebrafish. Dev Dyn. https://doi.org/10.1002/dvdy.24411

100. Reig G, Pulgar E, Concha ML (2014) Cell migration: from tissue culture to embryos. Development 141(10):1999–2013. https://doi.org/10.1242/dev.101451

101. Rangarajan S, Madden L, Bursac N (2014) Use of flow, electrical, and mechanical stimulation to promote engineering of striated muscles. Ann Biomed Eng 42(7):1391–1405. https://doi.org/10.1007/s10439-013-0966-4

102. Guo Y, Jardin BD, Zhou P, Sethi I, Akerberg BN, Toepfer CN, Ai Y, Li Y, Ma Q, Guatimosim S, Hu Y, Varuzhanyan G, VanDusen NJ, Zhang D, Chan DC, Yuan GC, Seidman CE, Seidman JG, Pu WT (2018) Hierarchical and stage-specific regulation of murine cardiomyocyte maturation by serum response factor. Nat Commun 9(1):3837. https://doi.org/10.1038/s41467-018-06347-2

103. Lee EJ, Holmes JW, Costa KD (2008) Remodeling of engineered tissue anisotropy in response to altered loading conditions. Ann Biomed Eng 36(8):1322–1334. https://doi.org/10.1007/s10439-008-9509-9

104. Huang Y, Zheng L, Gong X, Jia X, Song W, Liu M, Fan Y (2012) Effect of cyclic strain on cardiomyogenic differentiation of rat bone marrow derived mesenchymal stem cells. PLoS ONE 7(4):e34960. https://doi.org/10.1371/journal.pone.0034960

105. Maul TM, Chew DW, Nieponice A, Vorp DA (2011) Mechanical stimuli differentially control stem cell behavior: morphology, proliferation, and differentiation. Biomech Model Mechanobiol 10(6):939–953. https://doi.org/10.1007/s10237-010-0285-8

106. Rørth P (2009) Collective cell migration. Annu Rev Cell Dev Biol 25(1):407–429. https://doi.org/10.1146/annurev.cellbio.042308.113231

107. Mayor R, Etienne-Manneville S (2016) The front and rear of collective cell migration. Nat Rev Mol Cell Biol 17(2):97–109. https://doi.org/10.1038/nrm.2015.14

108. te Boekhorst V, Preziosi L, Friedl P (2016) Plasticity of cell migration in vivo and in silico. Annu Rev Cell Dev Biol 32(1):491–526. https://doi.org/10.1146/annurev-cellbio-111315-125201

109. Young JL, Engler AJ (2011) Hydrogels with time-dependent material properties enhance cardiomyocyte differentiation in vitro. Biomaterials 32(4):1002–1009. https://doi.org/10.1016/j.biomaterials.2010.10.020